Materials Science and Engineering and
Chemical Engineering Department

Master Thesis

Influence of the grain size and phase content on the mechanical behaviour of magnesium alloys. Gravity casting and SPS manufactured

Author: Juan Guillermo Santos Macías

Daily supervisor: Andrea Gil Santos

Tutor: Elisa María Ruiz Navas

Leganés, October 2015

Título: Influence of the grain size and phase content on the mechanical behaviour of magnesium alloys. Gravity casting and SPS manufactured (Influencia del tamaño de grano y la composición de fases en la respuesta mecánica de aleaciones de magnesio. Fabricación por fundición en molde permanente y SPS)

Autor: Juan Guillermo Santos Macías

Director: Elisa María Ruiz Navas

EL TRIBUNAL

Presidente: _____

Vocal: _____

Secretario: _____

Realizado el acto de defensa y lectura del Proyecto Fin de Carrera el día 30 de octubre de 2015 en Leganés, en la Escuela Politécnica Superior de la Universidad Carlos III de Madrid, acuerda otorgarle la CALIFICACIÓN de:

VOCAL

SECRETARIO PRESIDENTE

Acknowledgements

I would like to thank Andrea Gil Santos for her patience, advice and support. I also appreciate the help provided by Professor Omer Van der Biest, Professor Kim Vanmeensel, Professor Jozef Vleugels, Íñigo Marco, Thomas Lapauw, Karel Lietaert, María Montero, Paul Crabbé, Wout Veulemans, Pieter L'hoëst, Joop van Deursen and the rest of the staff at KU Leuven.

The adventure that was the collaboration between Universidad Carlos III de Madrid (UC3M) and Katholieke Universiteit Leuven (KU Leuven) would not have been possible without the cooperation of Professor Elisa María Ruiz Navas and Professor Nele Moelans. I am grateful for having had access to the facilities at KU Leuven and the MTM department as a visiting scholar.

This research was supported by funds from the People Programme (Marie Curie actions) of the European Union's Seventh Framework Programme FP7 (2007-2013) under REA grant agreement No 289163. This covered material, SEM hours, maintenance and training.

Resumen

El interés por los materiales biodegradables ha aumentado significativamente en los últimos años. En el contexto de los implantes óseos y las endoprótesis vasculares ("stents"), el magnesio, biocompatible, destaca sobre el resto de materiales. Siendo el metal estructural más ligero, su resistencia específica es sobresaliente. Su densidad y propiedades mecánicas son parecidas a las del tejido óseo, por lo que se evita la aparición de osteoporosis proximal que se debe a la transferencia de cargas a través del implante por diferencia de rígidez.

La baja resistencia a la corrosión del Mg provoca fallo mecánico prematuro en la prótesis e inflamación del tejido circundante debido a la acumulación de gases. Es necesario utilizar otros elementos biocompatibles a modo de aleantes para mejorar la resistencia a la corrosión y el comportamiento mecánico. El calcio, el manganeso y el estroncio son nutrientes esenciales que, incorporados en pequeñas cantidades, reducen el tamaño de grano y la velocidad de corrosión, aumentando la resistencia mecánica.

Mediante cálculos termodinámicos se predijeron y determinaron las composiciones más favorables de las aleaciones. Se llevó a cabo el estudio de muestras fabricadas por colada en molde permanente a partir de los sistemas Mg-Ca-Mn, Mg-Sr-Mn y Mg-Ca-Sr-Mn con el objetivo de determinar su potencial como materiales biomédicos. La microestructura y las fases presentes fueron caracterizadas. Se correlacionaron los resultados obtenidos en ensayos de dureza y compresión con el tamaño de grano y la naturaleza y cantidad de fases.

Se exploró una vía alternativa de producción mediante pulvimetalurgia. El sistema Mg-Ca-Mn fue escogido para esta tarea debido a las propiedades ventajosas del calcio. El proceso, consistente en una primera etapa de aleación mecánica para obtener un polvo de calidad seguida de sinterización por plasma pulsado, fue optimizado.

Palabras clave: Implante biodegradable; Magnesio; Manganeso; Calcio; Estroncio; Cálculos termodinámicos; Fundición en molde permanente; Aleación mecánica; Sinterización por plasma pulsado; Comportamiento mecánico; Compresión; Dureza; Tamaño de grano; Fases; Optimización

Abstract

The interest in biodegradable materials has significantly increased in recent years. In the context of bone implants and vascular stents, biocompatible magnesium stands out as a unique option. As the lightest structural metal, it has outstanding strength to weight ratio with density and mechanical properties close enough to those of bone tissue to avoid stress shielding.

Poor corrosion resistance of Mg leads to premature mechanical failure of implants and inflammation of surrounding tissue due to hydrogen gas accumulation. Alloying using biocompatible elements is needed to improve corrosion and mechanical behaviour. Calcium, manganese and strontium are essential nutrients that, added in low quantities, induce grain refinement, corrosion resistance and strengthening of Mg.

Thermodynamic calculations were used to predict and determine favourable alloy compositions. Gravity cast samples of Mg-Ca-Mn, Mg-Sr-Mn and Mg-Ca-Sr-Mn systems were studied to determine their potential as biomedical materials. Characterization of microstructure and phases was carried out. The mechanical data obtained from hardness and compression tests were linked to grain size and phase content and nature.

Exploration of a powder metallurgy manufacturing route was performed. The Mg-Ca-Mn system was chosen for this task, owing to the beneficial properties of calcium. Mechanical alloying to produce quality powder was followed by spark plasma sintering. The process was optimized.

Keywords: Biodegradable implant; Magnesium; Manganese; Calcium; Strontium; Thermodynamic calculations; Gravity casting; Mechanical alloying; Spark Plasma Sintering; Mechanical behaviour; Compression; Hardness; Grain size; Phase content; Optimization

Index

Index of abbreviations & symbols

ICP-OES	*Inductively Coupled Plasma-Optical Emission Spectroscopy*
XRD	*X-ray Diffraction*
SEM-EDS	*Scanning Electron Microscopy-Energy Dispersive X-ray Spectroscopy*
PM	*Powder Metallurgy*
SPS	*Spark Plasma Sintering*
HV	*Vickers Hardness*
wt%	*weight percent*
RE	*Rare Earth*
HA	*Hydroxyapatite*
BSE	*Back Scattered Electron*
FEA	*Finite Element Analysis*
UCS	*Ultimate Compressive Strength*

Index of figures

Index of tables

Chapter 1

Introduction & objectives

1.1 Introduction

Magnesium has proved to be a very interesting metal with a huge potential and numerous applications. Its attractiveness is mainly due to good mechanical properties and, perhaps more importantly, a very low density compared to other metals. Mg, with a density of 1.74 g/cm^3, is much lighter than titanium (4.51 g/cm^3) and even significantly less dense than aluminium (2.7 g/cm^3) [1].

As a light metal Mg is of great interest in industries such as the automotive, aerospace, etc. where reduction of weight is directly connected with lower fuel consumption. This was the main driving force for the start of Mg technology and since then increasing interest on Mg and Mg alloys has taken place in both industry and research domains.

In the case of biomedical applications, one of the most appealing advantages of using Mg is its biodegradable nature. Mg degrades when it is in contact with body fluids and it can be naturally resorbed by the human body without leaving trace of its presence in the organism. This is a very interesting feature in the case of implants that have to be removed after the healing process. The need to get rid of an implant once it has completed its task in the human body requires an extraction surgery. This intervention can not only prolong recovery time, but it could also represent a potential albeit minimal life threat in some cases. Medical expenses are also increased. A Mg implant would

ideally degrade during the healing process to the point where it would disintegrate and disappear completely. Thus, the extraction surgery would be avoided.

During the first steps of the healing process the implant has to be able to absorb loads and efforts that normally go to the part where the implant is now located. There should be a compromise between the degradation or corrosion rate of the implant and the recovery time of the healing part (a human bone). Mg corrosion becomes a crucial parameter and Mg implants present a significant disadvantage due to their low corrosion resistance. This material degrades at a rate that may cause deterioration of the implant mechanical properties before the end of the healing process. As a result, the implanted part cannot meet the mechanical requirements.

The use of alloying elements is a possible way to help decrease the corrosion rate. The sole action of alloying can also enhance mechanical properties. If the correct alloying elements are added in a convenient percentage corrosion behaviour can be greatly improved.

Great care must be taken, however, when choosing the alloying elements, especially in the case of biomedical applications. Even elements that are considered common and are not usually seen as a threat can be harmful to the human body. Such is the case of aluminium, as it is explained in the next paragraph.

In the case of implants, the problem of stress shielding has led to a search for alternative materials to steel, titanium and Co-Cr based alloys, which differ too much in mechanical properties (chiefly Young's modulus) from those of bone tissue [2]. Lightweight metals, such as Al and Mg, come out as a possible solution. Due to its low density and good mechanical properties, Al has lately increased in popularity in many fields. However, its application in the medical sector has recently been compromised. It has been reported that Al could be related to Alzheimer’s disease [3-5]. Due to this drawback, Al cannot be used as an alloying element for Mg in this case despite the fact that these two elements have been used together very successfully in other applications.

Therefore, in the search of alloying elements biocompatibility and non-toxicity are mandatory. To achieve this, a logical approach is to use elements that are naturally present in the human body, thus reducing risk of rejection and intolerance.

The ideal selected alloying elements have to improve Mg properties, but it also has to be taken into account that the biological nature of the applications asks for biocompatible elements. If these elements are naturally present in the human body, deleterious cell proliferation and thrombosis ocurrence would be avoided or significantly diminished.

Considering both their biocompatibility and their potential to improve mechanical properties, Ca, Mn and Sr are very good alloying candidates [6].

Ca is involved not only in essential functions but also in bone regeneration processes [7]. The human adult body contains about 1100g of Ca, nearly 1.5% of the body weight, and 99% of the total body Ca is contained in the skeleton. Ca is an indispensable element that performs essential functions in bone structures [7]. Mn is essential for cartilage synthesis and also reduces corrosion rate via transforming impurities into harmless intermetallics [4]. Sr promotes bone formation, diminishes bone resorption and increases

trabecular bone volume. In fact, it has been observed that Sr stimulates bone formation in rats [8]. Sr is a group 2 element that behaves similarly to Ca and can be commonly found as a Ca substitute in biomedical compounds such as hydroxyapatite [8,9].

Those three elements can improve the mechanical properties of the alloys and/or facilitate the production process. Ca can help in grain size reduction; when added to Mg above the solubility limit of 1.34 wt% Ca in Mg, the intermetallic Mg_2Ca forms; this compound will be located in grain boundaries [10]. Within Mg alloys, Mn reduces grain size and improves tensile strength and elongation [4] and Sr can increase the compressive strength and reduce surface tension of Mg, improving the castability [11].

Several systems made out of the selected elements have been studied, two ternaries, Mg-Ca-Mn and Mg-Sr-Mn, and the quaternary Mg-Ca-Mn-Sr, to determine their microstrucutre, phase composition and mechanical properties. The occurring secondary phases are composed of Mn and intermetallics Mg_2Ca and $Mg_{17}Sr_2$ [6]. These intermetallic compounds, formed by the interaction of the highly active Mg with the alloying elements, are of great importance. Their dislocation pinning properties and ability to annul grain boundary sliding can be very useful in mechanical behaviour improvement. They can also improve and refine microstructure [12].

This thesis is part of the MagnIM project, which seeks to develop Al-free Mg implant materials. MagnIM comprises three phases: Materials design and development; in vitro experiments; in vivo tests. The present work belongs to the first phase [13].

1.2 Objectives

The main objective of this thesis was to characterize different as cast samples of the Mg-Ca-Mn, Mg-Sr-Mn and Mg-Ca-Mn-Sr systems in order to establish a relation between grain size, phase content and mechanical properties depending on the alloying elements.

The second objective was to explore an alternative manufacturing process. Powder metallurgy (PM) is a very interesting and promising field. It could be convenient for biomedical applications, especially considering the relative small size of implant parts. Mechanical alloying followed by Spark Plasma Sintering (SPS) were performed in this work. Feasibility was studied and the production processes were optimized based on their parameters (milling time, temperature, applied pressure, etc.).

The final objective is to compare the thermodynamic calculations with the experimental results. Namely, for each system, the predicted and present intermetallic phases and their quantity are studied.

Chapter 2

Literature review

2.1 Material selection

In recent years the interest in lightweight materials has experienced a significant increase. Low density parts are seeing more applications in many sectors, especially in transport related ones, such as the automotive, with the intent of reducing energy consumption. In this context, composites and polymers are in vogue due to their lightness. Nevertheless, when superior mechanical properties are needed, metals -not iron (ρ = 7.87 g/cm^3), titanium (ρ = 4.51 g/cm^3) or copper (ρ = 8.96 g/cm^3), which are heavy, but aluminium (ρ = 2.7 g/cm^3) and magnesium (ρ = 1.74 g/cm^3), with especially low densities- appear to be the best choice. Mg in particular is very attractive because of its good strength-to-weight ratio, better than that of Al or steel [1,14].

Considering, for instance, the aerospace industry and its high and specific requirements, the importance of light metals is evident. The Airbus A380, the world's largest passenger aircraft, incorporates Al alloys in its structure, accounting for 61% of it (followed distantly by composites (22%)) [15]. As for Mg, it was already extensively used in the 1949 Convair B-36 bomber, containing 9500 kg of this metal [11].

In the automotive sector, weight reduction is preferentially achieved via material substitution. Redesigning and downsizing are the second and third main options, the former being less effective and the latter not appearing attractive to costumers due to loss of comfort. Hence, Al and Mg are gradually replacing the heavier steel components. Al is

used in engine blocks and wheels, while cast Mg has many potential applications as can be appreciated in figure 1, especially in thin walled parts [14].

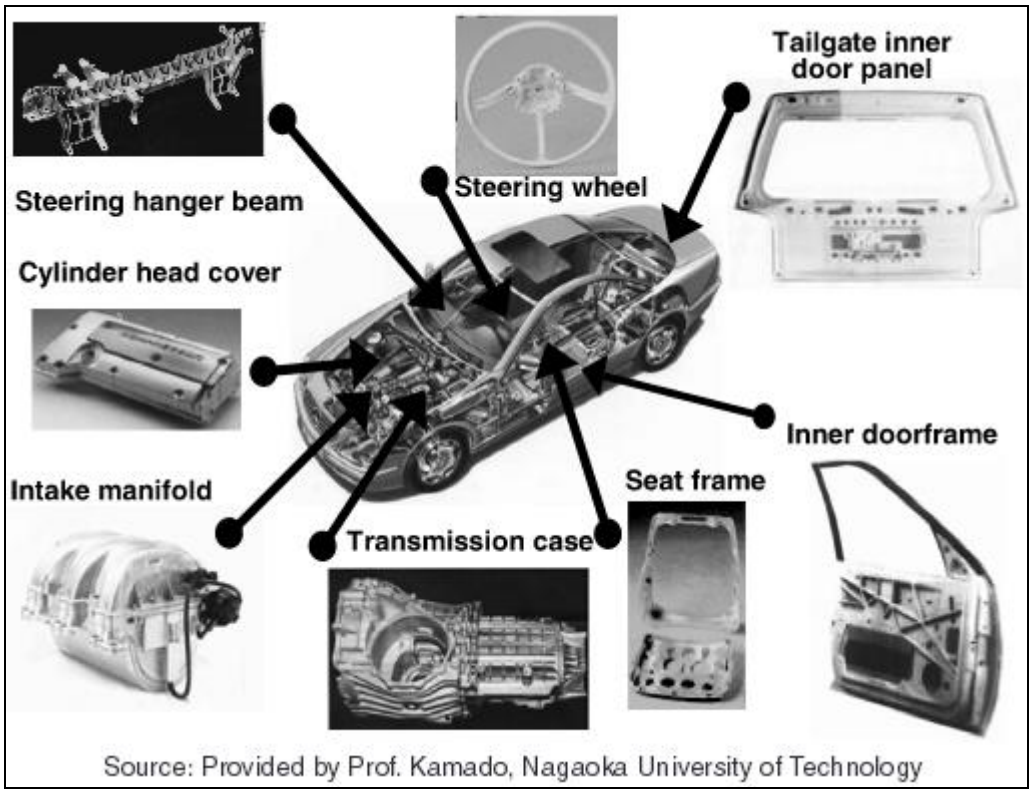

Figure 1: Mg in automobile parts [16]

The expertise acquired in a certain field is often transferred to others, implementing the necessary adjustments. The aerospace and automotive are two greatly competitive sectors, with very high standards. It would therefore seem advantageous to try to extract materials, manufacturing methods and know-how from these areas and adapt them to serve biomedical purposes, such as implant manufacturing. However, bioengineering has even stricter and particular requirements, so the conversion cannot be as direct as desired. Chiefly, toxicity has to be taken into account very seriously.

In implants, there are two main approaches to tackle the toxicity issue. The first one, which has been the trend for decades, is to use inert materials with superior corrosion resistance that ideally would not release harmful substances [3]. At first this appears to be the most adequate solution, but it is inconvenient in some ways. The inactivity can lead to lack of interaction and make it difficult for proper cell attachment and adequate implant-tissue interface growth to occur. Osseointegration is compromised. Stress shielding can also be an important concern [2]. The need for surface design and coating treatments ensues [17].

The other approach is to promote and exploit the biocompatibility aspect. Stimulating the interaction between the implant and the tissue better connection is achieved. The implanted part, which is a foreign body, becomes integrated. The discontinuation that exists between implant and tissue is smoothed. Mechanical load bearing will be facilitated.

In any case, achieving perfect biocompatibility is virtually impossible. This can result in infection, inflammation and implant rejection. The patient can experience pain, which can become chronic (especially in permanent implants), significantly decreasing quality of life.

In an effort to devise an adequate implant material, more biocompatible elements and alloys were used. Focusing on bone implants, the properties of this tissue were studied and those materials that matched them more closely were favoured. In this context, Mg appears as a goog candidate. Moreover, Mg has a feature that is normally considered a disadvantage, but in the biomedical field can be pretty useful.

A bone fracture may require orthopedic surgery, typically involving pins, rods, screws and/or plates implantation to set the damaged tissue for subsequent healing. The invasiveness of the procedure can vary depending on the extent of the injury. Nevertheless, an operation is always an ordeal, and, especially in the case of vulnerable individuals (e.g. elderly people), it implies certain risk. Furthermore, extraction surgery is commonly needed once the healing process is over and the implant parts have served their purpose.

Using Mg implants the extraction surgery can be avoided. This constitutes a very significant advantage, not only in patient safety and comfort but also from an economic viewpoint. Thanks to its biodegradable nature, a Mg implant will gradually corrode, being reabsorbed and substituted by new tissue, to the point where it will completely disappear.

It is therefore logical for Mg to be central to the recent enthusiasm for biodegradable metals [3]. However, this biodegradation process in Mg is normally too fast, the implant part loses its mechanical integrity before it has accomplished its task. The required mechanical strength is not met and the part fails before the healing process is over. Hydrogen gas produced in the corrosion process can also accumulate in the tissues, producing inflammation [2]. Hence, there is a need to alloy Mg with other elements that will decrease its corrosion rate.

This issue has been known for a long time. There are reported experiments with Mg implants from as early as the end of the nineteenth century. In fact, back then they were more popular than their Fe counterparts and saw numerous potential applications [3]. However, stainless steel development made it more attractive than Mg. The new inert materials were favored over Mg since the corrosion process control of the latter was not mastered at the time [18]. This was a serious setback to Mg alloys development in bioengineering. It was coupled with the regression produced by World War II (with loss or destruction of significant research progress in this field) and abandonment of Mg development in other strategic sectors (chiefly the arms industry) after the end of the conflict. Furthermore, in Germany, as the defeated side, a ban on Mg production was imposed [11]. All this entailed a serious blow to Mg biodegradable implants from which recovery took decades, since only recently has the practical use of these materials become again a realistic possibility, and this at a fairly primal level, with a lot of basic work still to be done.

In conclusion, it can be said that, although there are several options when choosing a material for biomedical implant applications, it is clear that metals have the longest

history in this sector (see figure 2) [19]. Thus, metal based materials, being more developed, can be presumed to be the best candidates to meet a certain set of requirements. More specifically, for bone implants and coronary and vascular stents, the capacity to bear mechanical loads is paramount. However, mechanical properties of the implant should not vary greatly from that of the surrounding tissue to avoid deleterious stress shielding phenomena. In this attempt at mimicking properties, density should also be taken into account (Natural bone density ranges between 1.8 and 2.1 g/cm^3) [2]. On the other hand, to avoid extraction surgery, pain and implant rejection issues, biodegradable materials are preferred when the application allows their use.

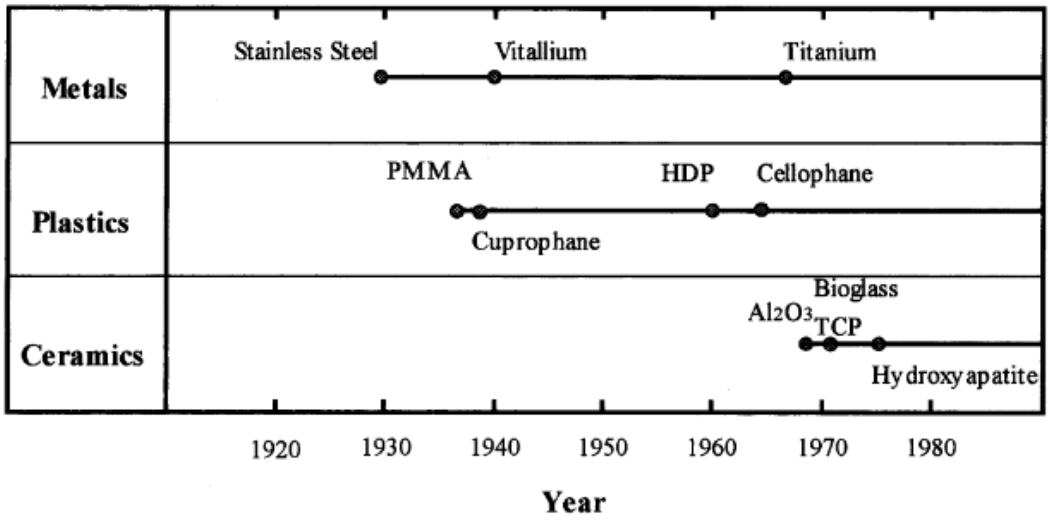

Figure 2: Timeline featuring the inception of different materials use in bioengineering [19]

Taking all this into account, Mg alloys emerge as the best possible choice. They have a low density, 1.74-2.00 g/cm^3, very similar to that of bone, 1.8-2.1 g/cm^3. Their elastic moduli (41-45 GPa) are also adequate, only slightly higher than that of osseous matter (3-20 GPa). Other mechanical properties are also at convenient levels (Compressive yield strength: 65-100 MPa for Mg alloys vs. 130-180 MPa for bone. Fracture toughness: 15-40 MPam$^{1/2}$ for Mg alloys vs. 3-6 MPam$^{1/2}$ for bone), especially compared to other alloys used in bioengineering, such as stainless steel, Ti, Co-Cr or artificial hydroxyapatite based alloys, all with significantly higher densities and mechanical properties (which lead to stress shielding issues) [2].

2.2 Alloying elements

Going back to implementation into bioengineering of current know-how on Mg alloys, the logical procedure is to look for those alloys that are more popular and have high-end properties. These should provide at the very least a good starting point. The AZ91 alloy (9 wt% Al, 1 wt% Zn) is the most used in casting (which in turn is the most used manufacturing method) [20]. In other production processes different Mg alloys are utilized, such as AZ31 or AZ61 in forming [21]. More specialized or niche techniques have not been profoundly explored for Mg. For instance, in biomedicine, where the parts

are small and porosity can promote cell proliferation and osseointegration and serve as drug carrier, powder metallurgy (PM) could be an interesting possibility. Mg, although typically considered soft, is suitable for this method as it is hard enough to be milled at high speeds to produce the powder raw material [20]. With the proper alloying elements, PM can significantly enhance the appeal of Mg in bioengineering.

The presence of Al enhances mechanical and corrosion behaviour [4]. Many alloys contain rare earth (RE) elements, introduced in small percentages to improve creep resistance [20]. To increase ductility, Mn is added [21]. Other alloying elements are Ag, Ca, Li, Si and Zr [20].

It is thus apparent that Al and Mg go well together. And they should, since they are similar in several ways. They are next to each other in the periodic table, with atomic number 12 for Mg and 13 for Al. Despite their different crystal structure (hexagonal close packed (HCP) for Mg and face centered cubic (FCC) for Al), their similar size allows atomic substitution. Their melting points are also comparable at 660°C for Al and 650°C for Mg [1].

However, the biomedical context requires good biocompatibility. This is true for Mg, which plays a biological role in the human body, but not for Al. The latter is not required by animals or plants and, when present in the organism, accumulates in bone and nervous tissue [3]. It is suspected to be associated to neurotoxicity and Alzheimer's disease [3-5]. Consequently, despite its appeal, it cannot be considered for biomedical use.

Therefore, the alloying elements must be chosen with the utmost care. For instance, RE elements are also to be used with caution since they are difficult to obtain in a pure form. Moreover, Nd and Y have been found to cause problems in implant applications, while inadmissibly poor biocompatibility was detected for La and Ce [4,22].

On the other hand, it seems wise to utilize alloying elements that are naturally present in the human body and perform a biological role. In this way, the benefits of alloying are obtained without major toxicity issues. The following alloying elements were selected in this work according to these criteria:

Manganese (Mn): Experiments with this element have shown a significant decrease in grain size, especially in extruded alloys (e.g. AZ61), exhibiting its usefulness in usually necessary subsequent processes (e.g. forming, heat treatment) [23]. This, coupled with corrosion resistance enhancement via absorbing impurities, makes Mn a key additional alloying element (i.e. not normally used alone with Mg, but in addition to other alloying elements [24]. This achieves quality improvement of the compound), just as it is for steel [4]. It helps in improving mechanical behaviour while preserving ductility of Mg [11,25,26]. It is related to bone and enzymatic and metabolic processes, with a significant relevance to the point where Mn insufficiency is linked to osteoporosis, arteriosclerotic vascular disease and diabetes [3,4].

Calcium (Ca): Belonging to the alkaline earth metals, the same periodic table group as Mg, their numerous similarities point towards good compatibility. Addition of this element can help in the manufacturing process (including PM [27]) and produces a significant grain refinement effect [24]. Moreover, both Ca and Mg are essential

biological elements, not only for humans but for virtually any other organism. A small percentage of human Ca (1%) has missions in blood, cells and muscles [3]. More important is the well known role of Ca in bone tissue, forming part of the so called bone mineral, which is based on hydroxyapatite (HA), chemical formula $Ca_{10}(PO_4)_6(OH)_2$. HA and Mg-substituted HA formation will thus be enhanced around a Mg bone implant containing Ca, increasing corrosion resistance (if Ca content is kept below 1%) [24].

Strontium (Sr): This element also belongs to the same periodic table group as Mg and Ca, entailing similar properties. It reduces grain size. 99% of human Sr is found in bone tissue. It has a significant role in osseous processes. It induces bone healing through positive influence on osteoblast development (osteoblasts are the cells responsible for creation and growth of bone) and reduction of osseous resorption (this process is, in contrast, led by different cells, the osteoclasts). Such is its effectiveness that it is used to treat osteoporosis cases [3,24].

It is worth mentioning that multi-element alloys usually yield better results than binary alloys, with smaller total alloying content (in weight percentage). This is a well-known phenomenon referred to as the third element effect [6]. Thus, three or more elements are used to produce a compound. Two ternary and a quaternary systems were studied in this work (Mg-Ca-Mn; Mg-Sr-Mn; Mg-Ca-Sr-Mn). However, the study of the binary systems serves very well as a starting point. Information obtained from the more simple systems can be useful as a base for the more complex ones.

Figures 3 to 5 portray the Mg-Ca, Mg-Sr and Mg-Mn binary diagrams, obtained from Thermo-Calc software (using TCMG2 commercial database).

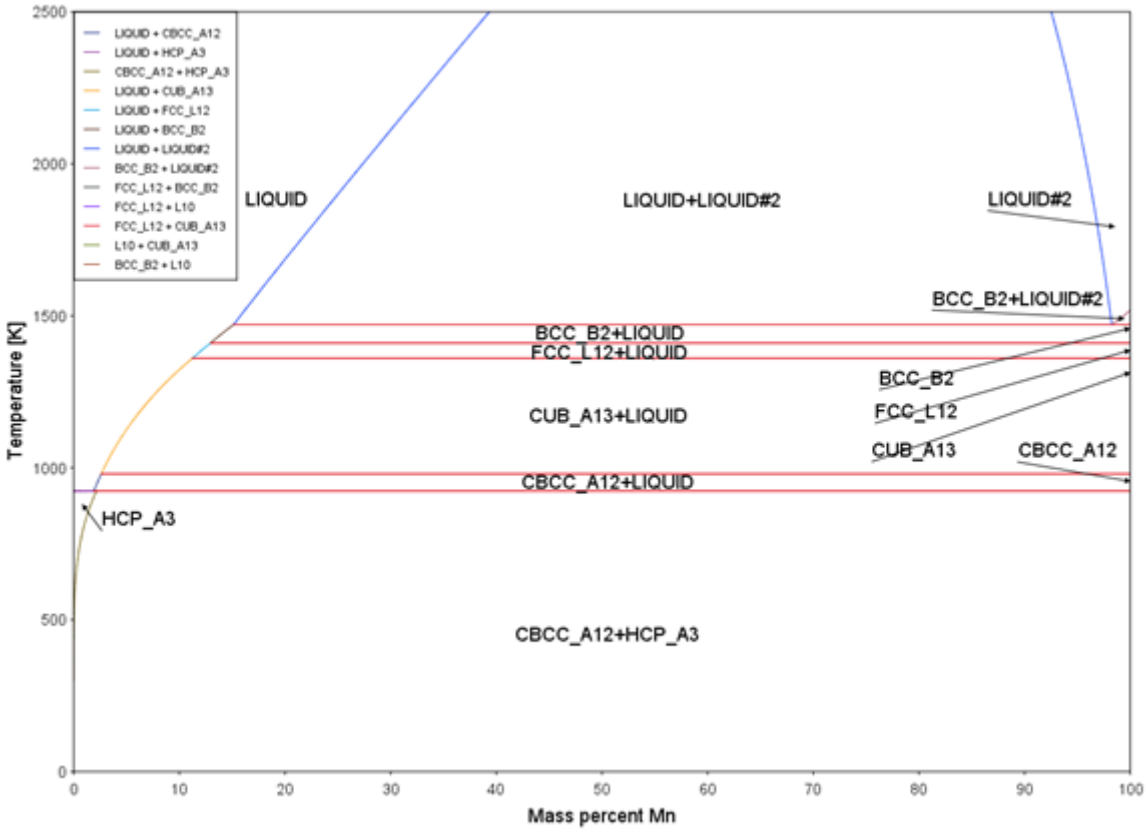

Figure 3: Mg-Mn binary diagram

A major part of the Mg-Mn diagram (figure 3) is governed by the peritectic transformation just above 650°C. Focusing on the left Mg-rich sector, it can be observed that with low content of Mn, direct solidification from liquid to Mg (HCP_A3 in figure 3) takes place. Thus the maximum solubility of Mn in Mg is 2 wt%. No intermetallics occur. The Mn that is not in solid solution is expected to be present alone in its typical body centered cubic crystal structure (CBCC_A12 in figure 3).

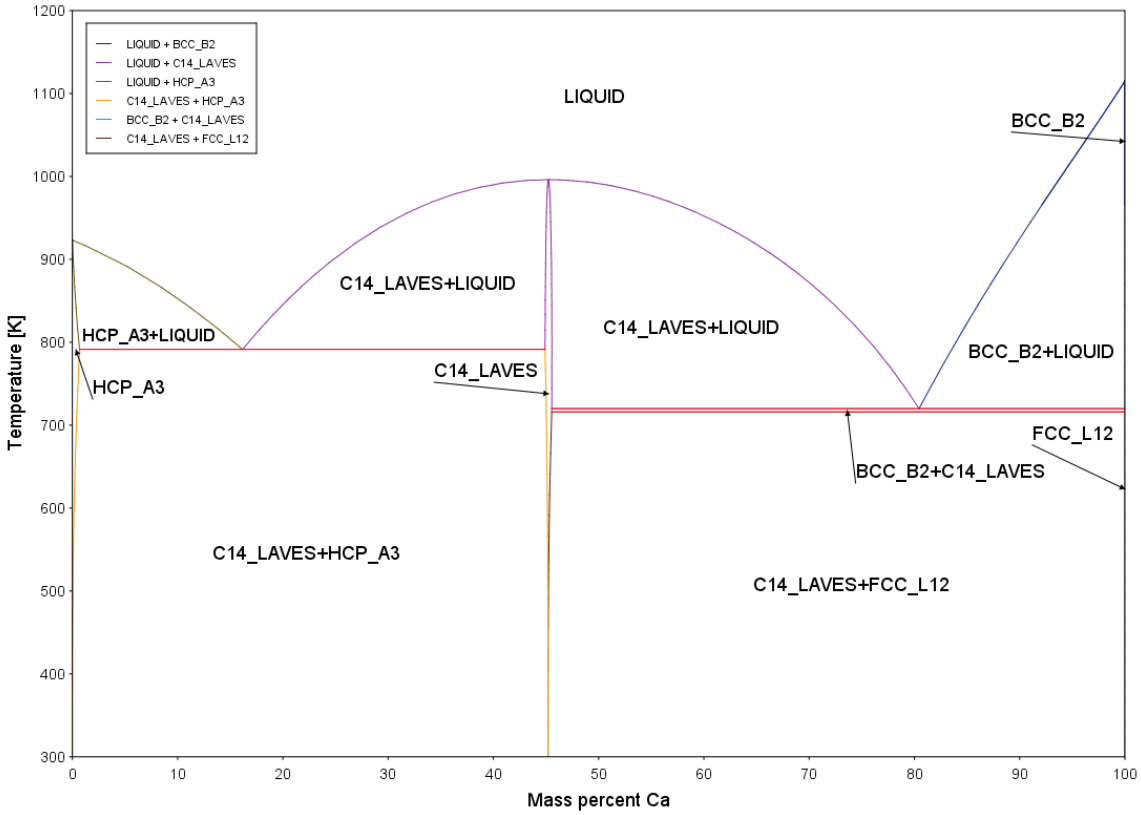

Figure 4: Mg-Ca binary diagram

The main feature of the Mg-Ca diagram (figure 4) is the Mg_2Ca intermetallic phase (C14_LAVES in figure 4), forming along grain boundaries. This interesting compound can enhance strength of Mg. However, if present in high amount the consequent ductility decrease (from cracks originating at the more brittle intermetallic) could be detrimental and corrosion resistance could be weakened [4]. Therefore, Ca content should stay low. The solubility limit of Ca in Mg is 1.34 wt%.

The Mg-Sr diagram (figure 5) is more complex, having several intermetallic compounds. Among them $Mg_{17}Sr_2$ is the relevant phase when dealing with low alloyed compositions, which precipitates on grain boundaries, increasing strength at the expense of ductility. Maximum solubility of Sr in Mg is particularly low at 0.11 wt%, diminishing the content needed to form the useful intermetallic.

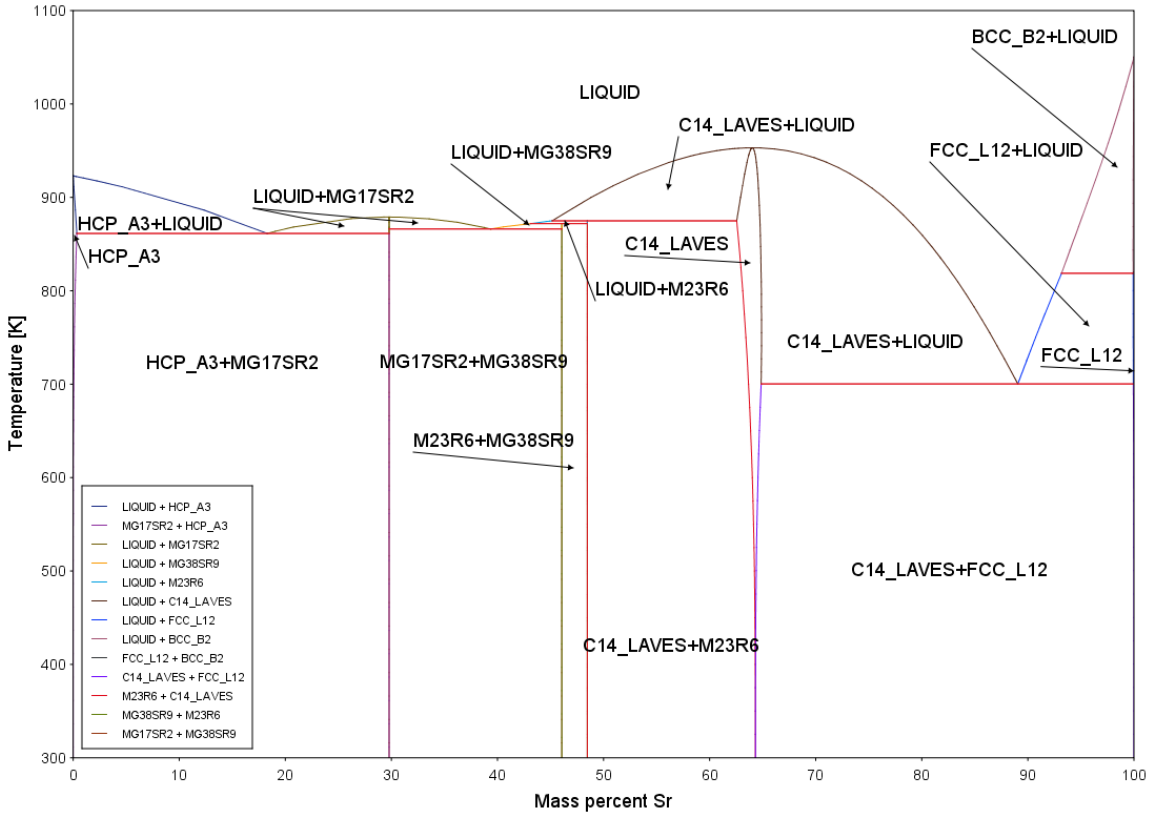

Figure 5: Mg-Sr binary diagram

The process of developing an alloy for biomedical implant purposes is far from simple. It is a multidisciplinary endeavour taking years of work. Practical Mg alloy implants are scarcely beginning to appear on the market, with very specific applications in concrete parts of the body. Research is still needed at all levels. However, patents have already been granted for the Mg-Ca-Sr system among others [28]. A few Mg alloys have recently seen application in humans and even commercial use [29].

Chapter 3

Experimental methods

3.1 As cast manufactured

3.1.1 Sample manufacturing

The samples were manufactured in the Magnesium Innovation Centre (MagIC) facilities, in Geesthacht, Germany. The rods were obtained via permanent mold gravity casting. The raw materials were pure Mg (99.95%) in ingot form, Ca (97.3%) chips, Sr (98.9%) flakes and master alloys (Mg10Ca, Mg2Mn, and Mg1Mn). Melting of these materials was done using an electrical resistance furnance with Ar and SF_6 as protective gases. When Ca chips where needed, they where preheated to 400°C and added to the rest of the material, which was already inside the furnace at 700°C (this temperature was reached in 40 minutes). After that, temperature was kept around 700-750°C for 45 minutes, stirring every 15 mintues to achieve uniformity. Then the melt was stabilized at 760°C and poured into a mild steel die coated with boron nitride (preheated to 400°C). The resulting ingots were cylinders with 18 mm diameter and 20 cm length. The cylinders were demoulded after 2 minutes and left to cool down at room temperature in order to get slow solidification (about 10°C/min) as close as possible to the equilibrium one.

The ternary systems Mg-Ca-Mn and Mg-Sr-Mn and the quaternary Mg-Ca-Mn-Sr are investigated in this work. Thirteen different compositions located in the Mg-rich corner of the systems were processed. Five of them belong to the Mg-Ca-Mn ternary

system. Another five rods were composed of Mg, Sr and Mn. The remaining three were Mg-Ca-Mn-Sr quaternary alloys. Additionally, two pure Mg rods were produced to serve as control.

Figure 6: Melt being poured into the mild steel die

Figure 7: Master alloys (top left corner) and gravity cast Mg alloy rods

3.1.2 Sample composition

The nature of the elements used for sample manufacturing and the particularities of the casting process, involving high temperatures, can lead to deviations so called burn-off from the intended composition. These deleterious effects were taken into account and measures were implemented into the process to counterbalance the deviations. An example of these measures is adding a significantly higher amount of Ca and Sr into the mould to compensate for the losses during heating.

An element analysis is then needed to determine the actual composition. Inductively Coupled Plasma-Optical Emission Spectroscopy technique (ICP-OES) was chosen for this purpose. The measurements are based on the comparison with standard curves previously calculated for the pure elements. X-ray fluorescence (XRF) was also considered and used as a fast method to get the approximate compositions. This step is highly adviced in order to get a good reference for the preparation of the standards. The

Varian 720-ES ICP optical emission spectrometer was used. This method consists on nebulising the previously dissolved material through an Ar plasma (acting as both the carrier gas and the plasma) in order to excite its atoms. The electrons absorb energy and the atoms change to an excited state. Energy of a determined wavelength is emitted when the atoms go back to the ground state. The measurement of the intensity (c/s) of this energy yields the elements concentrations (ppm) with which material composition can be calculated.

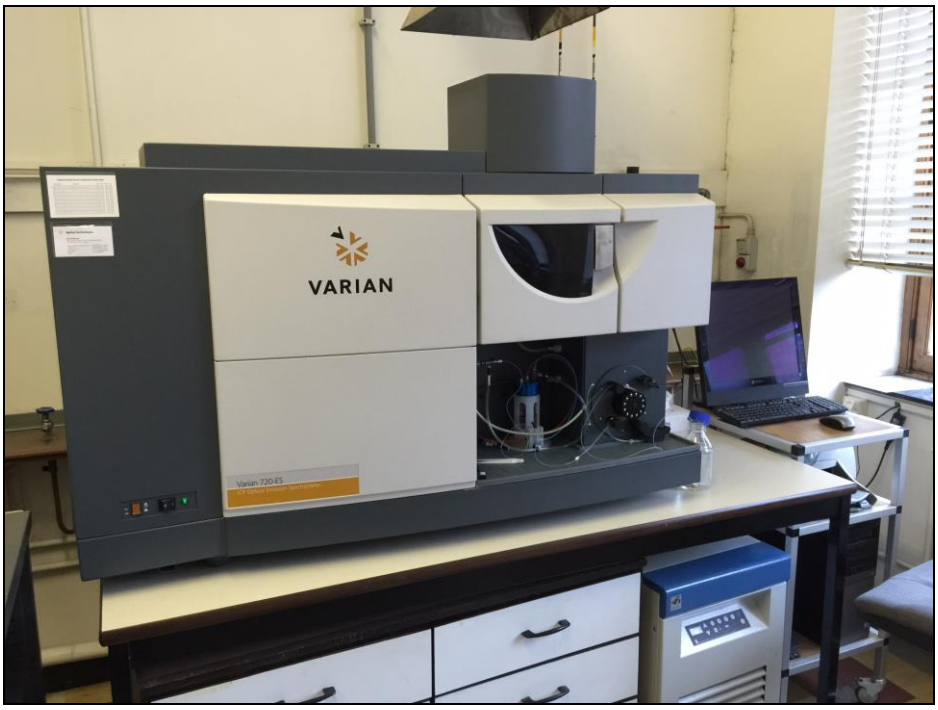

Figure 8: Varian 720-ES ICP optical emission spectrometer

In order to atomize the material it has to be in liquid form. Thus, the Mg alloys have to be first dissolved and, secondly, diluted, using HNO_3 and milli-Q water respectively.

The sample preparation process consisted in first retrieving a small piece of Mg alloy weighing 50 mg. It was then immersed in 3 mL of HNO_3 65% a.r., enough to achieve full dissolution. Finally it is diluted in milli-Q water up to the desired concentration.

The spectrometer needs at least 5mL of liquid to perform the analysis, so dilution is required to obtain sufficient amount. For this step the detection limits have to be taken into account (0.001-50 ppm for Mg, 0.003-150 ppm for Mn, 0.0003-15 ppm for Ca, 0.0002-10 ppm for Sr). Milli-Q water was used as diluent to avoid contamination. This very pure water was obtained with the Direct-Q 3 UV (with pump) water purification system, from Millipore S.A.S. 67120 Molsheim, France. Depending on the specific alloy, the final solutions ranged from 100 mL to 250 mL.

Figure 9: Direct-Q 3 UV (with pump) water purification system

Standard intensity vs. concentration curves or calibration lines had to be obtained to know what concentration corresponds to the measured intensity of each element in each sample. Four standard curves, one for each element, were needed. Each curve was plotted using four "known" points and making sure that the range was wide enough to include the expected concentration (i.e. composition) inside the interval set by the extreme points. To get these "known" points, standard solutions were made out of 1000 ppm base solutions of each element, adding milli-Q water. Since the concentration of these standard solutions is known beforehand, the intensitiy given by the spectrometer when one of these solutions is analysed can be linked to the concentration, establishing a relation (the standard curve). When the Mg alloy samples are later analysed, their composition is calculated by interpolating those standard curves.

3.1.3 Prediction and calculation of intermetallic phases

When designing alloyed materials for a certain application with a set of requirements, it is very helpful to have a way of determining the composition and percentage of alloying elements needed to meet the specific conditions. Knowing in advance what the microstrucutre and its components will be is also convenient.

Simulations using thermodynamic data can be used in this designing phase. These simulations are based on phase diagrams that provide the visual representation of the equilibrium state of a material as function of temperature, composition, pressure or any other viable state variable. This is the main reason why they are frequently used as a starting point for materials design and process optimization, tailoring compositions and variables in order to achieve the desired microstructures.

The construction of phase diagrams is based on the minimization of the Gibbs energy function, whose value has to be described for every single phase present in a multicomponent system [30].

For the better understanding of the metallurgical reactions and processing of materials the knowledge of the equilibrium state under applied conditions is of great importance. Thanks to phase diagrams and CALculation of PHAse Diagrams or CALPHAD method this information can be easily obtained.

Those calculations can significantly reduce experiments, saving time and resources. For instance, the correct percentage of alloying elements can be established and unwanted secondary phases can be avoided, allowing only the formation of those phases that will be beneficial in the manufactured parts.

In this project thermodynamic calculations were used to help decide the quantity of Ca, Mn and Sr added to Mg for the production of the samples. Thermo-Calc (versions 3.0.1 and 2015a) and Pandat (version 8.0) softwares were the two programs used for this purpose. The TCMG2 commercial database and an internally developed Mg-Ca-Mn database were utilized in Thermo-Calc and Pandat respectively. Later, experiments were performed to attest the accuracy of these predictions.

To see the solidifying path and the phases forming during solidification, Thermo-Calc was used, getting vertical sections. Together with isothermal sections, equilibrium final phase composition and phase percentages can be obtained.

Real solidification may differ from the one simulated in a vertical section since real solidification is a non-equilibrium process. To remedy this discrepancy, softwares like Thermo-Calc and Pandat offer the Scheil module where the Scheil-Gulliver model is applied. This model, the opposite case to the equilibrium solidification, assumes that the diffusion coefficients in the liquid phase are equal to infinity (considering fast diffusion in the homogeneous liquid phase) whereas in the solid phases they are equal to zero (no diffusion condition in the solid phases, during or after solidification). Because of this, Scheil solidification simulations were also performed. In fact, the real solidification path falls in between these two.

With the vertical section and Scheil solidification simulations a prediction of phase weight percentage can be obtained for the manufactured samples. These can be later compared with experimental data.

Pandat software is similar to Thermo-Calc, allowing to perform thermodynamic calculations, such as isothermal sections, vertical sections, Scheil solidification simulations, point calculations, etc.

Using the Pandat point calculation phase weight percentages were obtained for the Mg-Ca-Mn system only, since the database used in this program contains information for Mg, Ca and Mn, but not for Sr.

3.1.4 Sample preparation

Disk samples of 18 mm diameter and 2 mm height were cut from the central part of the cast rods.

Some experiments require a fine polished sample surface to be performed, namely the microscopy analyses, SEM and XRD. Therefore the disks were ground with 800, 1200, and 1200/4000 grit (the numbers correspond to the grinding paper roughness, a higher number meaning less roughness). They were further polished using water-free active Oxide Polishing Suspension (OPS) and 0.3 µm diamond slurry (manufactured by IDA Industriediamant-Aachen). For the samples that needed embedding, it was done before sample preparation using Demotec 30, a two component resin.

3.1.5 X-ray Diffraction (XRD) spectroscopy

For the identification of secondary phases in all the alloys, X-ray diffraction (XRD) was carried out in a XRD Seifert 3003-TT using Cu-Kα radiation at 40kV and 40 mA, from 10 to 80 degrees with a 0.02 step size. The identification of the phases was done by comparison with the phase patterns from the Joint Committee on Powder Diffraction Standards (JCPDS) cards included in the Pearson database. The used cards for Mg, Mg_2Ca, $Mg_{17}Sr_2$ and Mn are identified with numbers 00-035-0821, 01-073-5122, 03-065-3649 and 01-089-2412 respectively. The phase identification was always performed by analysing the results from polished as-cast samples at room temperature.

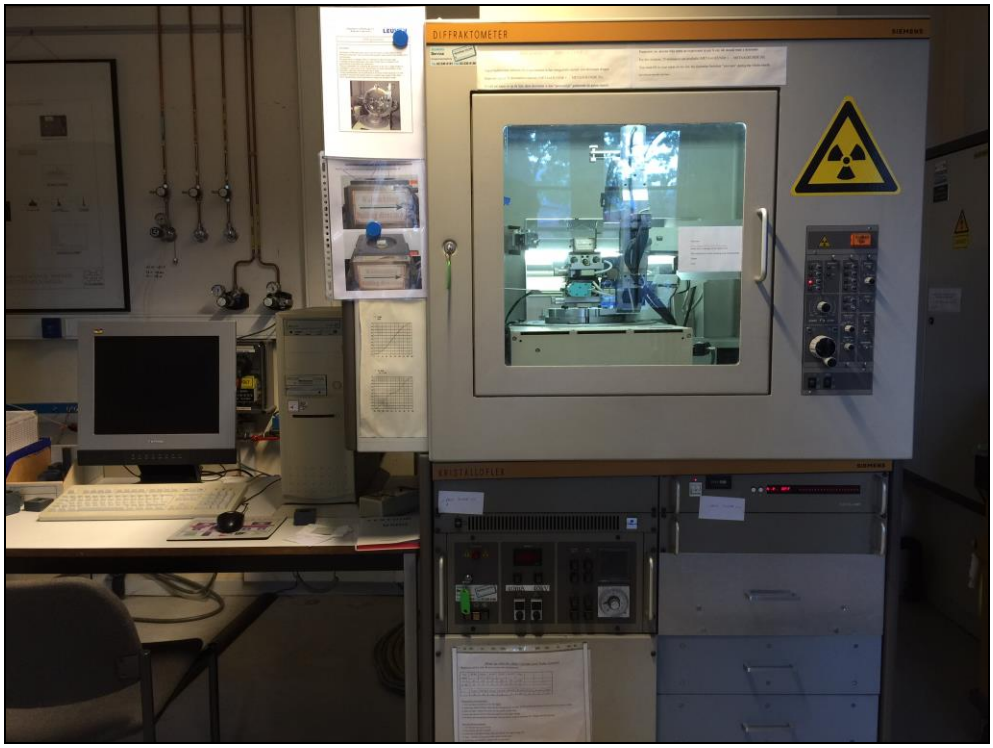

Figure 10: XRD Seifert 3003-TT and Siemens D500 goniometer

The obtained diffractograms were then compared with the ones in the reference cards to ascertain their presence and processed with a semi-automatic Rietveld refinement procedure [31] to get phase percentages, using the X'Pert HighScore Plus software.

3.1.6 Scanning Electron Microscopy (SEM) – Energy Dispersive X-ray Spectroscopy (EDS)

The microstructure was analysed using an optical microscope and a Philips XL30 FEG scanning electron microscope (SEM) equipped with an EDAX TSL energy dispersive X-ray spectroscopy (EDS) detector. Backscatter electron (BSE) images were used to identify the stoichiometry of the compounds.

The phase volume fractions were measured by image analysis of the micrographs using ImageJ 1.49p image processing program. For that, the SEM micrographs obtained with the Back Scattered Electron (BSE) mode were used. The image method provides values in volume percent and they were transformed into mass percent in order to make them comparable with calculations. For these calculations phase densitites were needed. They can be calculated for instance with the data provided in the phase pattern references mentioned in the previous section. The following formula and table respectively depict the way of calculating density of the phases belonging to the Mg-Ca-Mn-Sr quaternary system present in the studied samples and the phase data:

$$\rho = \frac{Z \cdot M}{V_{cell} \cdot N_A} \quad [\, g/cm^3]$$

Table 1. Phase data

Phase	**Mg**	**Mg_2Ca**	**Mn**	**$Mg_{17}Sr_2$**
JDPS card number	00-035-0821	01-073-5122	01-089-2412	03-065-3649
Crystal structure	Hexagonal	Hexagonal	Hexagonal	Cubic
Lattice parameters (Å)	a=b=3.2094 c=5.2112	a=b=6.2528 c=10.1435	a=b=10.5330 c=10.3420	a=b=c=8.9125
V_{cell} (10^6 pm^3)	46.48	343.45	707.94	993.66
Z (atoms/unit cell)	2	4	58	2
Density (g/cm^3)	1.736	1.715	7.474	1.967

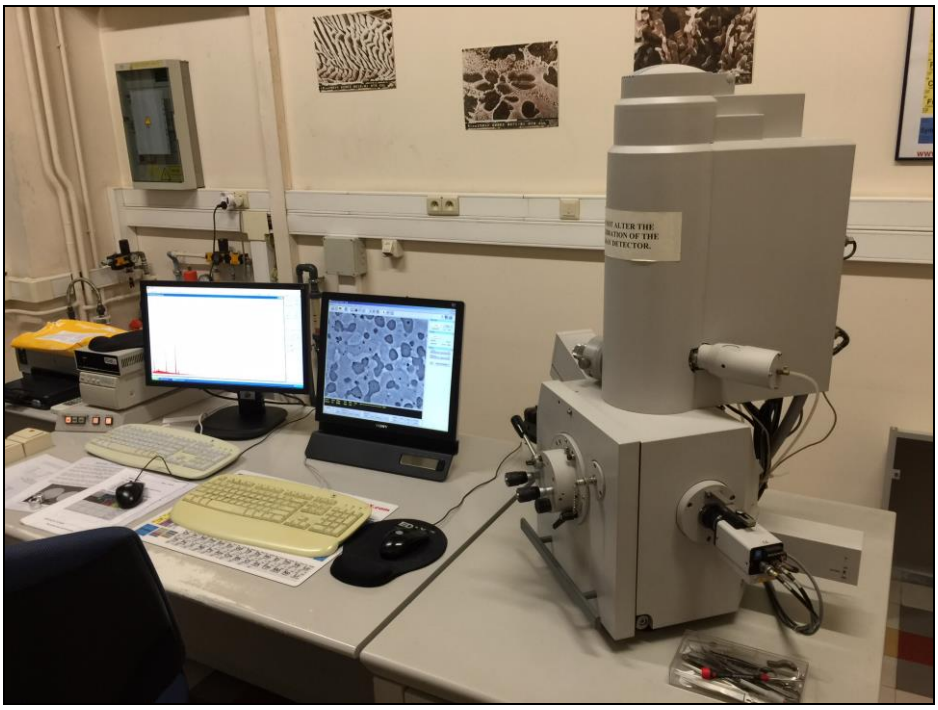

Figure 11: SEM XL30 FEG microscope

3.1.7 Etching, microstructure

Microstructure analysis was done as well with an optical microscope. Zeiss axiovision LE software was used to acquire micrographs of the sample surface. The optical micrographs were taken after etching the previously polished surface in order to easily reveal the microstructure. The etching agent used was picric acid based, containing 10 mL of acetic acid, 4.2 g of picric acid, 20 mL H_2O and 50 mL ethanol and the etching time was between 5 and 10 seconds. The average grain size was measured with Image-Pro Plus 6.0 image processing software from optical microscope images from the etched surfaces. The linear intercept method was used.

3.1.8 Vickers Hardness (HV)

Due to the relative softness of the material, to obtain information about hardness of the samples a microhardness test was needed. Vickers hardness (HV) was obtained with a Durimet microhardness tester (Leitz GmbH, Wetzlar). The following parameters were used: weight 25 p (i.e. 25 gf or 245.2 mN) and confidence limit of 0.95. Samples were polished before testing and placed plane-parallel to the indenter.

The test consisted in making indentations on the surface of the disc sample with the microhardness tester, equipped with the diamond tip shaped in a 136° square-based pyramid form that is required for the Vickers hardness testing method. Thanks to the camera implemented in the tester microscope the size of the indentation can be determined. With that a hardness value is acquired. Five indentations are performed for each sample, calculating the arithmetic mean and its error.

Figure 12: Durimet microhardness tester

3.1.9 Compression

It must be taken into account that the main stresses experienced by bones are due to compressive loads. Considering then the intended application of the alloys, compression tests were performed. The test was done following standard methodology [32].

Cylindrical compression test samples of 6 mm diameter and 10 mm height were electro discharge machined (EDM) from the as cast rods.

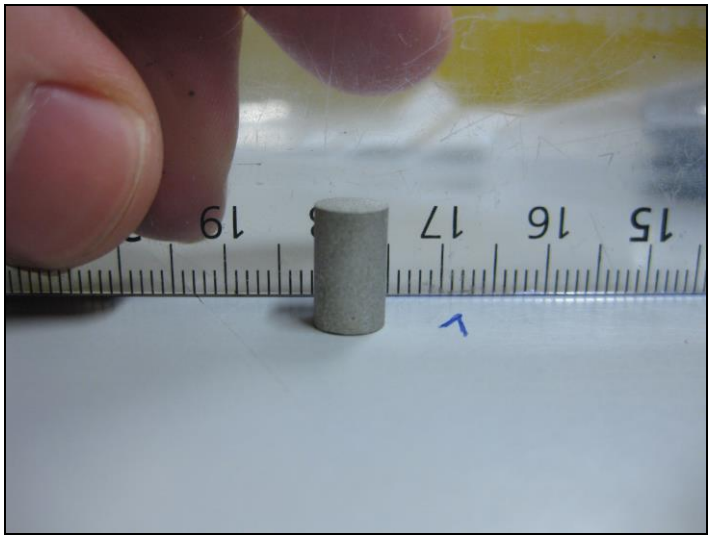

Figure 13: Compression specimen

An Instron 4467 materials testing tensile or compression system was used to perform quasi-static (0.5 mm/min) simple compression tests until failure. Load was applied

parallel with the axis of the cast cylinder and three to six compression tests were carried out per alloy. The machine was equipped with a 30 kN load cell. Teflon sheet was placed between the specimen to be tested and the bearing blocks as a lubrication measure. This reduces friction and the related barreling phenomenon which can influence the test.

3.2 Mechanical alloyed and SPS manufactured

An alternative manufacturing method not involving melting is powder metallurgy (PM). This unique feature allows for higher control and significant energy saving. It is especially adequate for biomedical applications where small and intrincate parts are needed. Furthermore, it must be noted that, although the occurrence of porosity in PM can be an issue in some cases, in the bioengineering field taking advantage of this feature is possible. Even open porosity can be beneficial in implant parts. A porous surface can promote osseointegration. Pores can also serve as drug receptacles or reservoirs (e.g. antibiotics, painkillers) that could enhance tolerance (decreasing implant rejection) and help in the healing process [27].

Normally PM comprises two differentiated steps, compaction of the powder (pressure is applied) followed by sintering (heat is applied). Compaction produces the "green part", a packed powder piece with low porosity but high brittleness. The sintering step binds the particles together by atomic diffusion, further reducing porosity and greatly increasing the previously poor mechanical properties.

In this project the Spark Plasma Sintering (SPS) was used. It combines the compaction and sintering steps into a single heat and pressure stage. This yields several advantages, among which time saving is notable. The work done previously by other authors was considered to design and optimize the mechanical alloying [33-38] and SPS processes [27,39-43].

Since the materials employed are very reactive (particularly Mg) and prone to oxidation in air (especially Ca and Sr), Argon was used to protect them during handling and manufacturing. A glovebox was utilized to create this protective atmosphere.

3.2.1 Material obtention

Mechanical alloying was performed to obtain a good quality powder for the SPS. The raw material for the mechanical alloying process was in the form of turnings, chips or granules. The initial materials were a slab of Mg (cut out of a 99.9 wt% purity Mg ingot (KBM Affilips, Tienen, Belgium)) and Mg10Ca and Mg2Mn master alloys (Magnesium Innovation Centre MagIC, Geesthacht, Germany). Turnings were obtained from these initial pieces by drilling.

Note: 99.5 wt% purity Ca granules (3.35 mm diameter) from Chempur were first used as mechanical alloying raw material, but the results were not satisfactory since some

of the granules did not break completely into fine powder. The Mg10Ca master alloy yields better results.

Sr poses some challenges to this manufacturing method. It is highly reactive, even more than Mg or Ca, and pyrophoric in powder form, igniting at room temperature in air. Considering the potential safety risk, the manufacturing was limited to the Mg-Ca-Mn system. Furthermore, it is not easy to obtain a convenient source of Sr. The hazard this element constitutes translates into fewer product range and supply and higher purchase price (e.g. when shipped from the USA, this material must be delivered via freight forwarder, with a minimum 1000$ cost). Table 14 in appendix illustrates the market survey done for the preliminary study of the possibilities of the powder metallurgy path.

3.2.2 Mechanical alloying

The turnings obtained by drilling were milled into powder or mechanically alloyed with a PM 400 MA-type planetary mill (Retsch GmbH, Haan, Germany). The mill was loaded with zirconia (ZrO_2) vessels containing 5mm diameter zirconia balls (milling media), material turnings and around 5 wt% stearic acid (95% purity, Sigma-Aldrich) in between the balls and the turnings to act as lubricant. ZrO_2 vessels and balls were used instead of more common steel ones to avoid contamination. This alloying process was done under Argon atmosphere to avoid oxidation.

Figure 14: Opened PM 400 MA-type planetary mill (left) & Powder product (right)

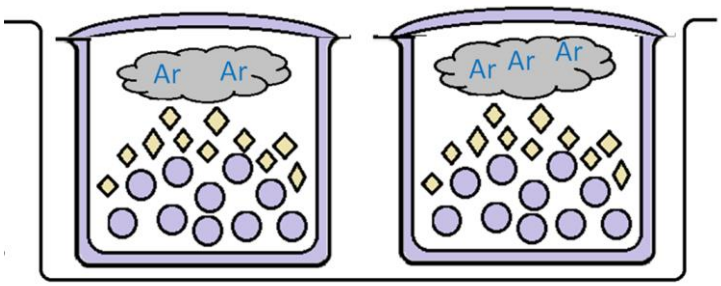

Figure 15: Schematic drawing of the zirconia vessels containing the ZrO_2 balls (in purple), the stearic acid (white crystals), the Ar protective atmosphere and lids to keep the system closed

Due to the fire hazard of this manufacturing step, derived from the high oxidation potential of Mg and the alloying elements, various milling speeds and times were used, analysing the result of each setting, size and shape of the powder, using SEM. Milling speed and time were gradually increased in order to limit risks during this tuning of the process.

When increasing the milling time a point was reached where the material stuck to the milling balls and the vessel wall (see figure 16). The cold welding and plastic deformation were predominant over the fracture process in this case. It was therefore clear that a compromise between speed, time and powder quality and size was needed and the obtention of those optimal values was intended with the first experiments.

Figure 16: Material stuck to milling media and vessel wall

Efforts were done to overcome this issue of material sticking to the balls and the vessel, aiming to reduce powder size without increasing milling time. An example of this was cryomilling. An attempt was made to implement it as an improvement to the process, to speed up the milling. The idea behind this method is to embrittle the material so it breaks down more easily [36]. It was performed by pouring liquid nitrogen into the vessel just before turning the planetary mill on.

3.2.3 Spark Plasma Sintering (SPS)

SPS is a powder metallurgy manufacturing method. It consists on simultaneously applying continuous current and uniaxial pressure to turn powder into a desired solid part. Joule heating and plastic deformation occurs in the material. The temperature is below the material's melting point but high enough to allow sintering to take place, producing atom diffusion and joining the particles together.

Figure 17: HPD 25 furnace (left) & Detail of the interior of the furnace (right)

An HPD 25 furnace from FCT Systeme (Rauenstein, Germany) was used for this step of the manufacturing process [44]. SPS was done under vacuum holding 500°C and 20 MPa during five minutes in a 30 mm diameter graphite die. The die was filled with varying amounts of powder ranging from 6 to 15 grams. Graphite paper was introduced between the sample and the die to act as insulating coating. The powder inside the die was pre-pressed at 15 MPa before going into the SPS furnace. The powders were sieved before being introduced in the die with a 500 µm sieve in order to have more homogeneous material. The sintering temperature was reached by preheating rapidly to 450°C and then heating at a controlled rate of 10°C/min up to 500°C (i.e. 5 min of controlled heating).

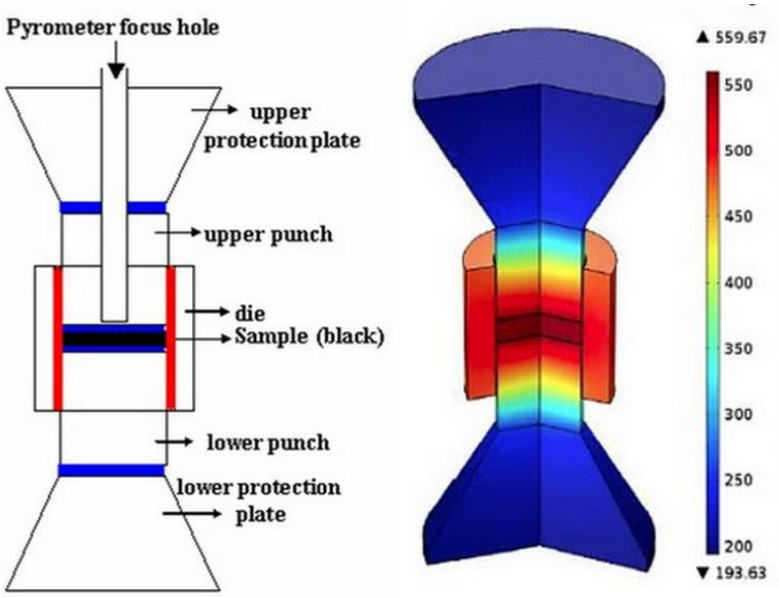

Figure 18: Diagram of the SPS arrangement (left) & FEA temperature distribution simulation (right) [44]

As indicated in figure 18 (left), the SPS machine has a measuring system that allows monitoring temperature from the top of the die, i.e. very close to the sample and the actual process. The expected temperature distribution inside the die was simulated using finite element analysis (FEA) as can be appreciated in figure 18 (right).

3.2.4 Density measurement

Due to the nature of the manufacturing process, porosity is always present in the final product. Achieving full density (this meaning above 95% density, which is considered closed porosity) through powder metallurgy is virtually impossible, so the aim is to get close enough to avoid a significant drop in mechanical properties. In the typical PM process, where compaction is followed by sintering in separated steps, porosity control is easier. Porosity reduction takes place mainly during compaction, sintering doesn't affect this property significantly. Seen from this perspective, SPS is more complex because the pressing and sintering steps cannot be clearly distinguished. A good porostiy level, that is a low level, would indicate that the process is well optimized.

Porosity of the samples was checked to establish the success of the production method. A way of doing this is to measure density, assuming previous data are available to compare with (e.g. the phase densities listed in table 1). Higher density and lower porosity indicate better process parameters.

Density of the SPS samples was determined using an Archimedes density measurement kit. With these data porosity can be obtained. The samples were weighed in air and ethanol. With the retrieved weights the density is calculated thanks to the following formula [45]:

$$\rho_{abs} = \frac{m_{air}(\rho_{liq} - 0.0012)}{0.999836(m_{air} - m_{immerse})} + 0.0012 \quad [\, g/cm^3]$$

In this formula $\boldsymbol{m_{air}}$ and $\boldsymbol{m_{immerse}}$ stand for the measured weight of the sample in air and ethanol respectively, while $\boldsymbol{\rho_{liq}}$ is the density of the ethanol used in the weighing. The digits in the formula are buoyancy related corrections.

Figure 19: Archimedes density measurement kit

Chapter 4

Results & discussion

4.1 As cast manufactured

The as cast samples were characterised, determining their composition, microstrucuture and mechanical properties. With these data the different samples and systems can be compared among each other. The specific application sets the required properties and, when applicable, their desired numeric value range, allowing ranking and discerning the suitability of each composition. In the case of bone implants, the properties of the human bone are the staple to attain in order to assure osseointegration.

The effect of the alloying elements on the properties and the dependence on composition variation is also important. Establishing relations or functions between amount of element and numeric value of a property is complicated, but can prove to be very useful. The studied materials can be used as implants in different parts of the body with varying requirements. Mg based alloys can also be used for coronary and vascular stents, requiring different properties.

4.1.1 Nominal vs. real composition

In the following table the differences between nominal and analyzed sample compositions can be appreciated:

Table 2. Nominal vs. ICP experimental composition (in weight %) for cast alloys

Nominal composition	ICP composition
Mg 0.24Ca 2.10Mn	Mg 0.45Ca 1.82Mn
Mg 0.24Ca 1.20Mn	Mg 0.21Ca 1.05Mn
Mg 0.18Ca 1.20Mn	Mg 0.17Ca 1.10Mn
Mg 0.60Ca 0.60Mn	Mg 0.52Ca 0.62Mn
Mg 1.60Ca 0.54Mn	Mg 1.49Ca 0.51Mn
Mg 0.57Mn 5.80Sr	Mg 0.51Mn 0.86Sr
Mg 0.57Mn 5.80Sr	Mg 0.64Mn 0.65Sr
Mg 1.30Mn 0.59Sr	Mg 1.27Mn 0.11Sr
Mg 0.65Mn 2.34Sr	Mg 0.73Mn 0.28Sr
Mg 2.20Mn 0.79Sr	Mg 1.86Mn 0.10Sr
Mg 1.30Mn 0.79Sr	Mg 2.21Ca 0.50Mn 0.17Sr
Mg 1.20Ca 1.10Mn 1.80Sr	Mg 1.26Ca 1.06Mn 0.30Sr
Mg 0.24Ca 0.6Mn 0.79Sr	Mg 0.31Ca 0.58Mn 0.16Sr

The most remarkable thing about these data is the significant loss of Sr in the casting process. The reactivity of this element makes its incorporation into the melt difficult. Part of it oxidizes and becomes slag at the top of the metal liquid. The slag, formed by impurities and oxides, is not poured into the mold, but removed when required after stirring the melt.

The low weight percentages of the alloying elements mean that the composition variation is very significant. A better control of the manufacturing process is needed, especially if medical or industrial applications are planned. That is why the method of mechanical alloying followed by sintering of powders is seen as an improvement in sample production. In contrast with casting, in SPS the material losses are minimized, making the final composition much closer to the intended one.

4.1.2 Microstructure

4.1.2.1 Grain size

During solidification, two competing phenomena occur, nucleation and grain growth. Alloying elements have a grain refining effect by inhibiting growth and promoting nucleation. They act as impurities where new grains can form, nucleation sites. As a result, more grain appearance events take place with higher amount of alloying elements.

The prevalence of nucleation over grain growth translates into higher number of grain boundaries, which hinder movement of dislocations. Mechanical properties, namely yield strength, are thus improved by a finer microstructure.

A fine microstructure is desirable, but the main grain refining effect is achieved with a fairly low percentage of alloying elements. Further alloying above this threshold will keep decreasing grain size, but it will do so at a much lower rate, up to a point where grain size will remain relatively constant [46,47]. Therefore, this alloying percentage should be kept to a minimum to avoid the disadvantages of increasing alloy presence. The

more complex and elaborated the material is, the more difficult it is to manufacture. Loss of cohesion and segregation are also issues in this case. After a certain level, the minor grain refinement inprovement brought by further increasing alloying content will not be worth the disadvantages.

Thanks to the etching process grain boundaries are revealed, as appreciated in figure 20, and can be distinguished with an optical microscope.

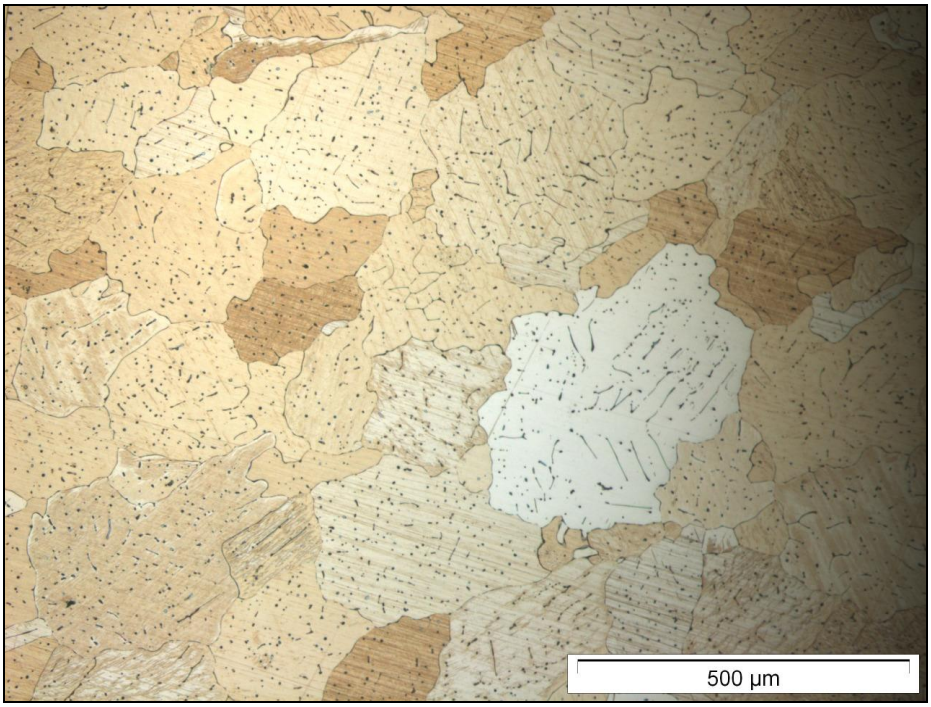

Figure 20: Grain boundaries on Mg 1.86Mn 0.10Sr sample

Images captured with Zeiss axiovision LE software were analysed using Image-Pro Plus, obtaining the following grain sizes:

Table 3. Grain size of cast samples estimated from etched surfaces with Image-Pro Plus software

Sample (wt% composition)	Grain size (µm)	Error %
Mg 0.45Ca 1.82Mn	217±113	52.1
Mg 0.21Ca 1.05Mn	333±237	71.2
Mg 0.17Ca 1.10Mn	189±116	61.4
Mg 0.52Ca 0.62Mn	224±125	55.8
Mg 1.49Ca 0.51Mn	54±36	66.7
Mg 0.51Mn 0.86Sr	102±68	66.7
Mg 0.64Mn 0.65Sr	106±81	76.4
Mg 1.27Mn 0.11Sr	99±62	62.6
Mg 1.86Mn 0.10Sr	131±87	66.4
Mg 0.73Mn 0.28Sr	182±153	84.1
Mg 2.21Ca 0.50Mn 0.17Sr	76±43	56.6
Mg 1.26Ca 1.06Mn 0.30Sr	143±60	41.9
Mg 0.31Ca 0.58Mn 0.16Sr	67±25	37.3
Pure Mg	132±45	34.1

Note: The grains of pure Mg samples are columnar (characteristic of ingot structure), so two dimensions have to be given to define them properly. The width is listed on the table, and the length is 2 or 3 mm or even more.

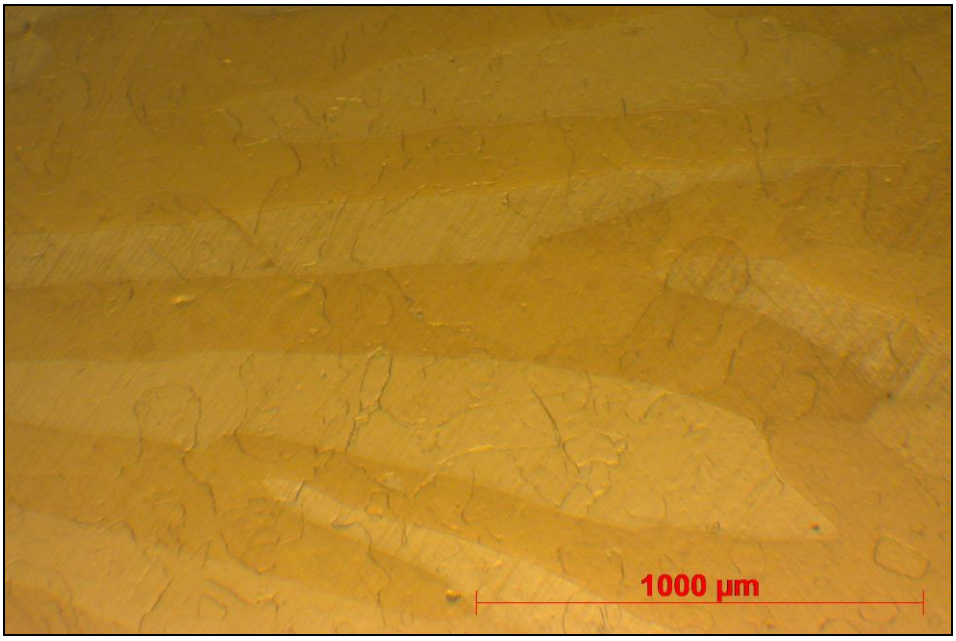

Figure 21: Pure Mg sample microstructure image

The microstructure of pure Mg disk samples can be seen with the naked eye (note scale on figure 21). The typical mold cast ingot crystalline structure with the presence of columnar grains can be appreciated. These are radial oriented growing grains following the temperature gradient. Pure Mg grains are significantly bigger than the ones in alloyed samples.

The deviation of the grain size values is significantly high. This is mainly due to the manufacturing process. In fact casting process produces non homogeneous grain size due to the relatively slow cooling rate, which permits significant grain growth. Comparison between the samples is therefore difficult. However, it is clear that alloying, even in low percentages, has a very important impact on microstructure. Not only does grain size decrease, but shape changes also. Grains become equiaxial instead of columnar, as seen in figure 22.

A few samples, chiefly the ones of Mg 0.21Ca 1.05Mn and Mg 0.17Ca 1.10Mn compositions, retain some columnar shape, especially in the edges of the discs, the areas that are far from the center. The grains are not as equiaxial as the ones found in other compositions. The ingot structure is still vaguely appreciable. This phenomenon can be explained looking at solubility of each alloying element in Mg.

Solubilities of Ca and Mn in Mg, 1.34 wt% [3] and 2.00 wt% [11] respectively, are relatively high in comparison to that of Sr, 0.11 wt% [3]. Thus, in the Mg-Ca-Mn system, lower alloyed samples have the majority of the alloying content in solution with Mg. Intermetallic secondary phases are almost absent. The contribution of alloying elements to grain refinement is in consequence significantly limited, although the main grain size reduction effect that occurs solely due to alloying is also taking place [46,47].

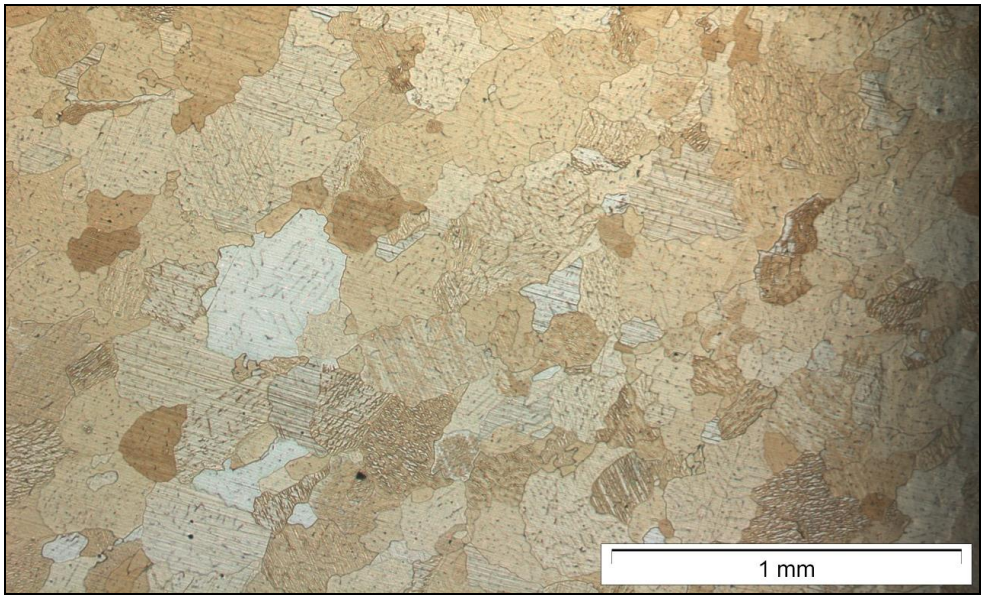

Figure 22: Microstructure image with equiaxial grains on Mg 1.86Mn 0.10Sr sample

Comparing the two ternary systems, Sr seems to have a more powerful grain refining effect, noticeable in figure 23. The effect of Mn is not clear, thus its influence seems to be somewhat less important.

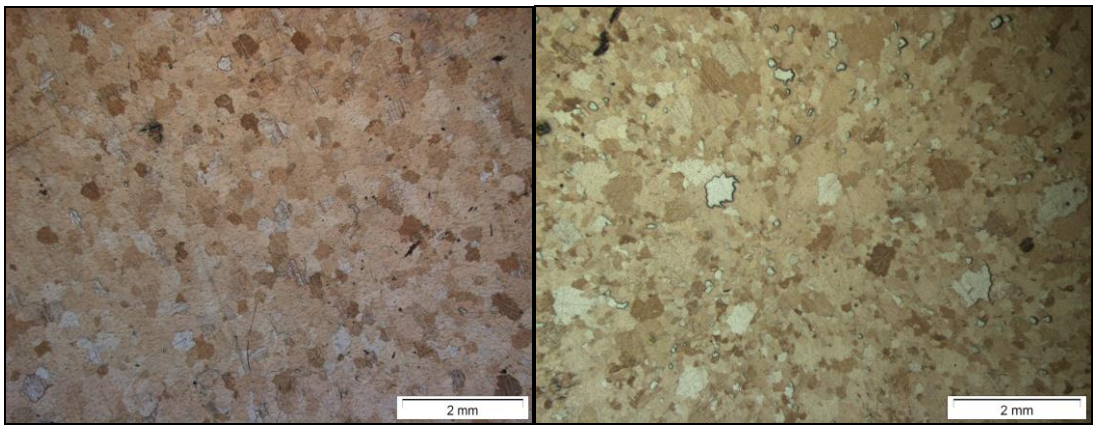

Figure 23: Comparison between Ca (left) & Sr (right) grain refining effect;
Mg 0.45Ca 1.82Mn (left) & Mg 1.27Mn 0.11Sr (right)

4.1.2.2 Phase presence identification

Isothermal sections of the different systems give information on the phases present in a certain composition. The following figures depict room temperature isothermal sections obtained with Thermo-Calc:

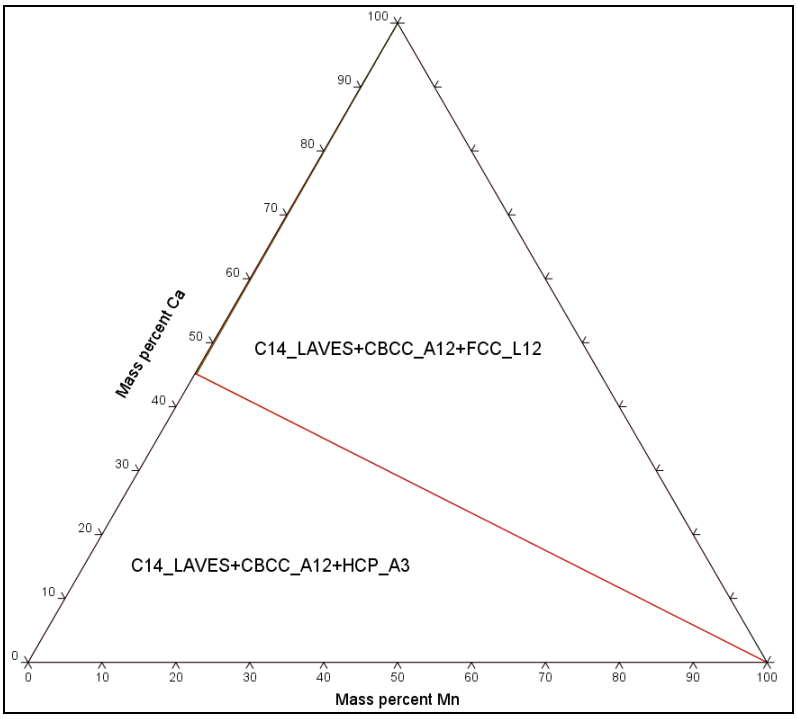

Figure 24: Isothermal section at room temperature of Mg-Ca-Mn

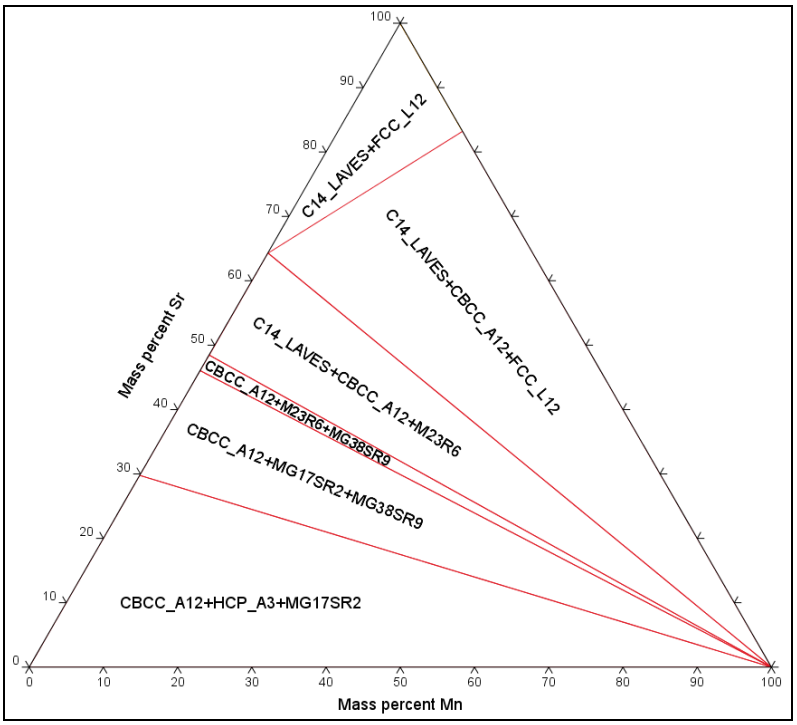

Figure 25: Isothermal section at room temperature of Mg-Mn-Sr

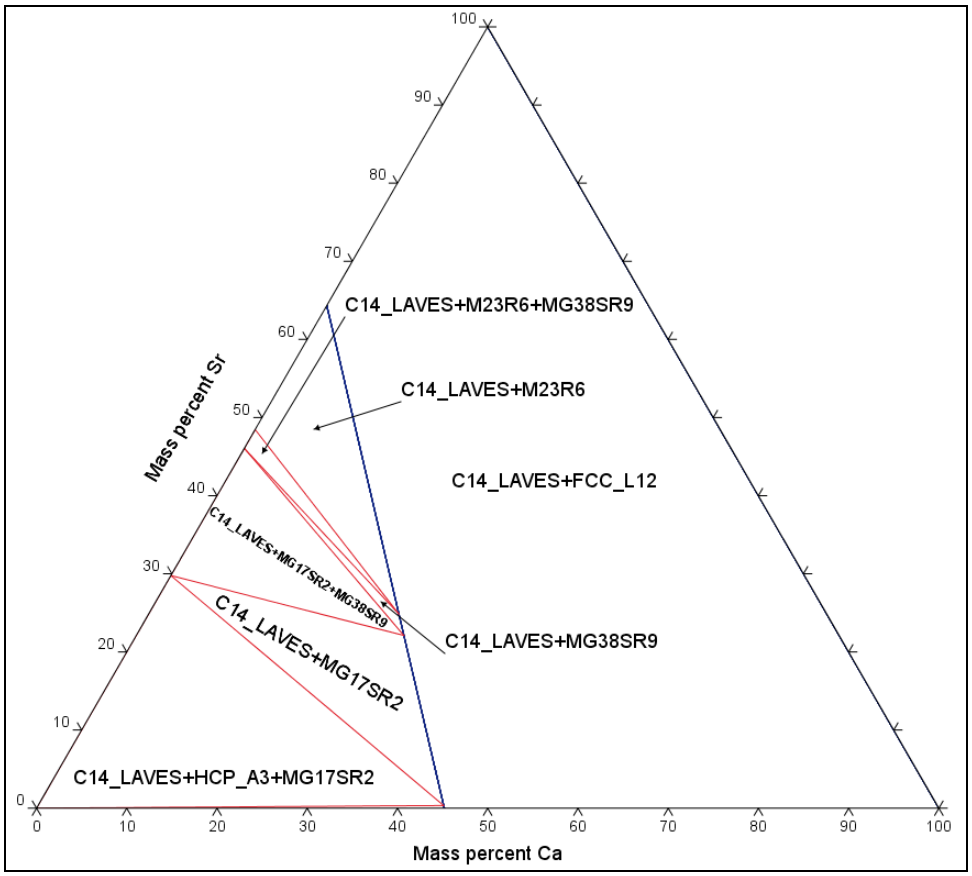

Figure 26: Isothermal section at room temperature of Mg-Ca-Sr

From these figures, focusing on the Mg-rich corner, it can be inferred that the expected phases in the Mg-Ca-Mn system samples are Mg (labeled HCP_A3 in the figure), Mn (CBCC_A12) and Mg_2Ca (C14_Laves). In the Mg-Mn-Sr system samples Mg, Mn and $Mg_{17}Sr_2$ are the phases predicted to appear. Finally, the isothermal section for the Mg-Ca-Sr system can be helpful to show the possible phases present in the Mg-Ca-Mn-Sr system. Considering Mn does not form intermetallic compounds with Mg, Ca or Sr, it does not add other phases than the ones appearing in the Mg-Ca-Sr system, exceptuating the pure Mn one. Mn will only occur as pure Mn secondary phase and in solid solution with Mg. Thus, for the quaternary system samples Mg, Mn, Mg_2Ca and $Mg_{17}Sr_2$ are the phases due to be present.

Further thermodynamic computation can include vertical sections with the corresponding solidification path of each composition. Although it must be noted that the real solidification differs from the equilibrium calculations, figures 42 to 44 in appendix can be used as a guideline.

These expected phases present in the samples can be confirmed with an analysis of the diffractograms obtained by XRD spectroscopy. The diffraction peaks of the samples were successfully linked with the ones in the Mg, Mg_2Ca, $Mg_{17}Sr_2$ and Mn phase patterns in the 00-035-0821, 01-073-5122, 03-065-3649 and 01-089-2412 reference cards (previously mentioned in section 3.1.5). Figures 27 to 29 depict diffractograms for each sample, ordered by system, with the peak identification.

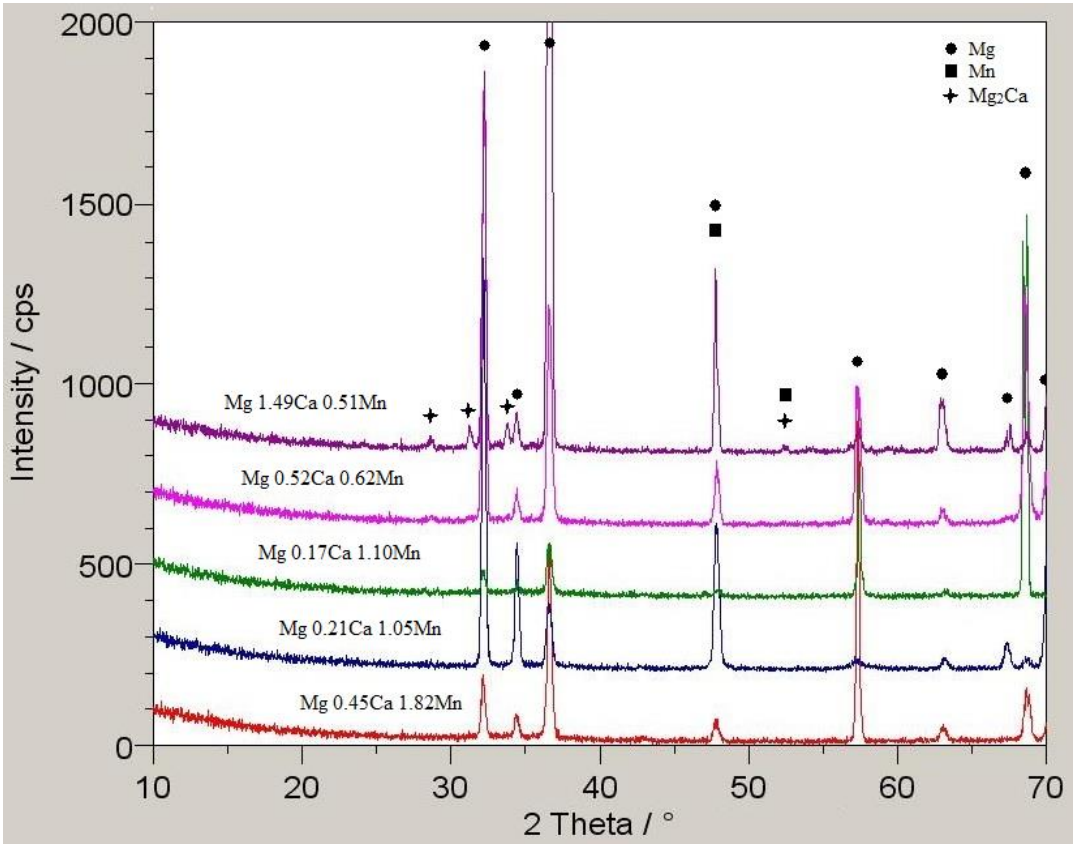

Figure 27: XRD patterns of Mg-Ca-Mn system samples

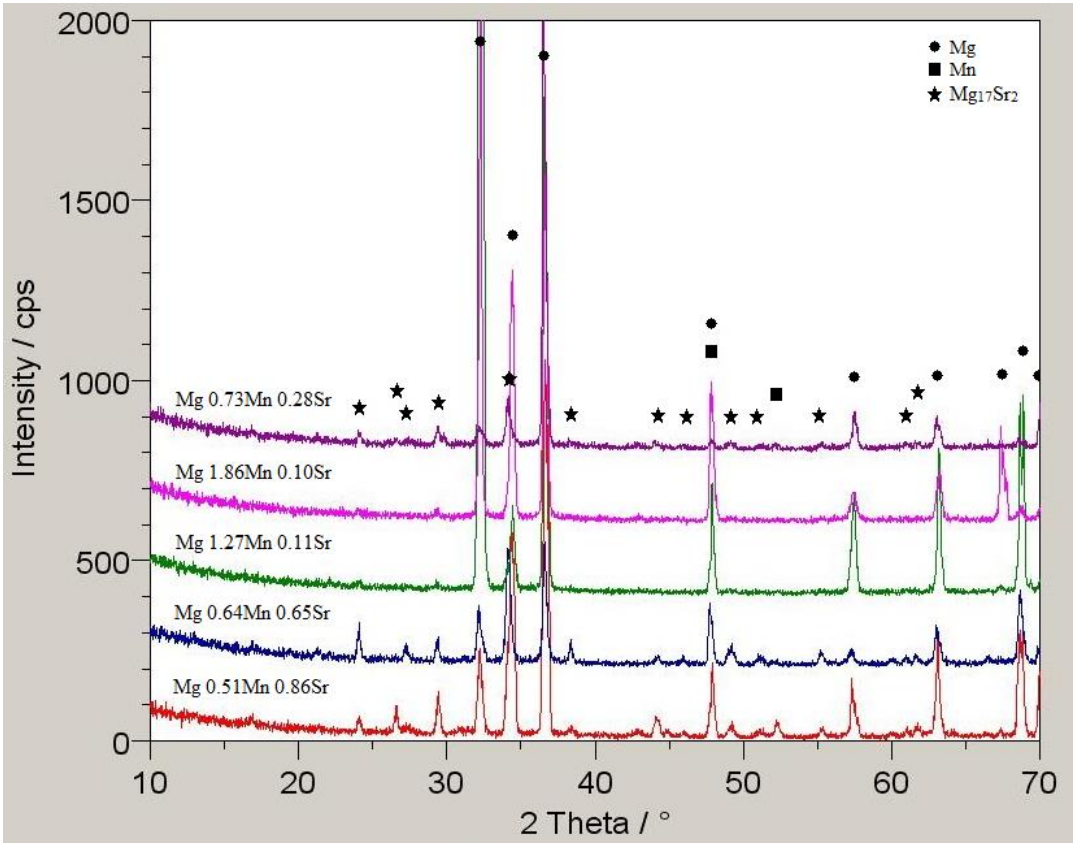

Figure 28: XRD patterns of Mg-Mn-Sr system samples

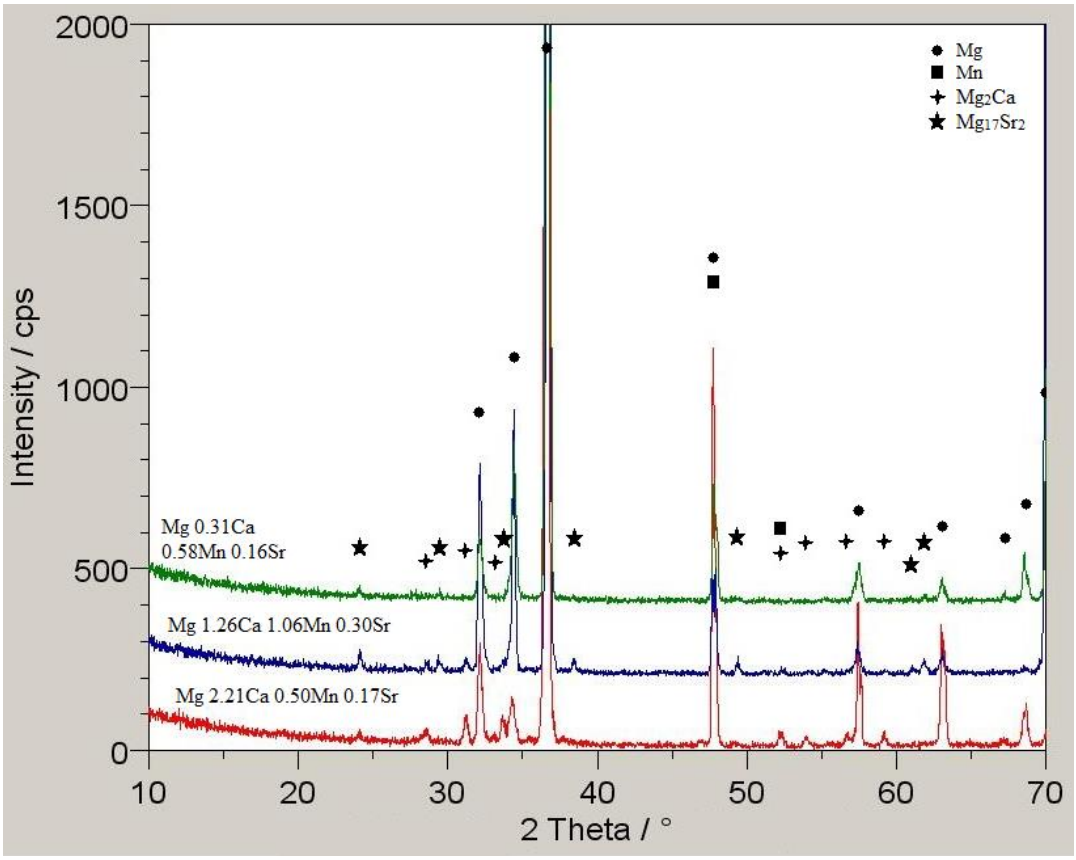

Figure 29: XRD patterns of Mg-Ca-Mn-Sr system samples

The SEM resolution allows to distinguish the different phases present in a sample (this can be appreciated on the SEM micrographs in figures 37 to 41 in appendix). Using the EDS detector equipped to the SEM, phase composition analyses were performed. These further confirmed the correctness of the phase presence predictions.

The SEM micrographs also show the phase morphology. Although the microstructure logically varies with composition, there are some common features to all. In the micrographs of figures 37 to 41, the darkest phase, the bulk, corresponds to the Mg matrix. It is composed of Mg with Mn, Ca and/or Sr dissolved in it. The other common trait is the presence of Mn particles, which are the brightest ones in the micrographs. These are composed solely of Mn and are distributed in a random manner all over the bulk and attached to secondary phases.

The other secondary phases are Mg_2Ca and $Mg_{17}Sr_2$. In the quaternary Mg 2.21Ca 0.50Mn 0.17Sr and Mg 1.26Ca 1.06Mn 0.30Sr, where both phases are present, they can be easily distinguished. Mg_2Ca has a eutectic structure, formed by Mg (darker) and Mg_2Ca (brighter in the micrographs). $Mg_{17}Sr_2$ is the solid, brighter phase.

In the other samples only three phases occur, so identification is easier. All phases are labelled in figures 37 to 41. It can be observed that, depending on the composition, a different solidification path is followed (see figures 42 to 44). Therefore, the morphology of Mg_2Ca and $Mg_{17}Sr_2$ will change. In some cases a eutectic structure forms (e.g. Mg 0.64Mn 0.65 Sr, where eutectic $Mg_{17}Sr_2$ forms from the liquid, precipitating in a lamellar structure of Mg and $Mg_{17}Sr_2$. This happens because when one of the phases begins to solidify from the liquid, the equilibrium is broken, so the other phase precipitates in turn until the equilibrium is broken once again and the previous phase solidifies again. This

process continues until the liquid is gone, forming the lamellae). In other cases a solid structure is formed, with no Mg interspersed (e.g. Mg 1.86Mn 0.10Sr, where $Mg_{17}Sr_2$ appears when there is no more liquid, so it forms out of the Mg phase that precipitated previously. No Mg forms at the same time and the resulting phase is that of solid $Mg_{17}Sr_2$ particles).

4.1.2.3 Phase fraction estimation

The phase fraction was estimated in the samples by three different methods. The obtained values where then compared in order to evaluate their reliability. Theoretical estimations of the values were calculated, using the Thermo-Calc and Pandat softwares with the previously mentioned databases. SEM micrographs were used to measure experimentally the amount of identified phases based on their different brightness and shapes. An image analysis software (imageJ 1.49p) was used. Finally a semi-experimental method was applied. Based on the experimental XRD patterns the fraction of intermetallic phases was calculated with the Rietveld refinement.

Thermodynamic calculations were used to predict phase percentages. Values were obtained with TCMG2 database in Thermo-Calc and Mg-Ca-Mn database in Pandat. The results coming from the Thermo-Calc software predictions are the mean between the equilibrium and Scheil solidification simulations. Point calculations were performed to get the Pandat data. Results for the different alloys are summarized in tables 4 and 5.

Table 4. Phase fractions (wt%) from Thermo-Calc (TCMG2 database)

Sample	**Phase fraction (wt%)**		
Composition in wt%	**Mn**	**Mg_2Ca**	**$Mg_{17}Sr_2$**
Mg 0.45Ca 1.82Mn	0.91	1.19	-
Mg 0.21Ca 1.05Mn	0.52	0.44	-
Mg 0.17Ca 1.10Mn	0.55	0.19	-
Mg 0.52Ca 0.62Mn	0.31	1.10	-
Mg 1.49Ca 0.51Mn	0.25	3.17	-
Mg 0.51Mn 0.86Sr	0.25	-	2.81
Mg 0.64Mn 0.65Sr	0.32	-	2.12
Mg 1.27Mn 0.11Sr	0.63	-	0.18
Mg 1.86Mn 0.1Sr	0.93	-	0.17
Mg 0.73Mn 0.28Sr	0.36	-	0.89
Mg 2.21Ca 0.50Mn 0.17Sr	0.25	4.79	0.26
Mg 1.26Ca 1.06Mn 0.30Sr	0.53	2.76	0.49
Mg 0.31Ca 0.58Mn 0.16Sr	0.29	0.57	0.26

Table 5. Phase fractions (wt%) from Pandat (Mg-Ca-Mn database)

Sample	**Phase fraction (wt%)**	
Composition in wt%	**Mn**	**Mg_2Ca**
Mg 0.45Ca 1.82Mn	0.81	0.83
Mg 0.21Ca 1.05Mn	0.47	0.38
Mg 0.17Ca 1.10Mn	0.49	0.31
Mg 0.52Ca 0.62Mn	0.27	0.95
Mg 1.49Ca 0.51Mn	0.23	3.29

The SEM micrographs were analysed with the ImageJ software to determine phase percentage. The utmost care was taken to analyse those micrographs that were as representative as possible, and several of them where analysed for the same sample. However, it must be noted that the manufacturing method can lead to segregation issues that could affect the accuracy of the analysis in some cases. The obtained data are presented in table 6:

Table 6. Phase fractions (wt%) from ImageJ analysis of SEM images

Sample	**Phase fraction (wt%)**		
Composition in wt%	**Mn**	**Mg_2Ca**	**$Mg_{17}Sr_2$**
Mg 0.45Ca 1.82Mn	0.19	0.80	-
Mg 0.21Ca 1.05Mn	0.15	0.02	-
Mg 0.17Ca 1.10Mn	0.26	0.28	-
Mg 0.52Ca 0.62Mn	0.14	0.82	-
Mg 1.49Ca 0.51Mn	0.13	6.08	-
Mg 0.51Mn 0.86Sr	0.19	-	10.18
Mg 0.64Mn 0.65Sr	0.13	-	12.00
Mg 1.27Mn 0.11Sr	0.11	-	1.75
Mg 1.86Mn 0.1Sr	0.16	-	2.00
Mg 0.73Mn 0.28Sr	0.05	-	4.95
Mg 2.21Ca 0.50Mn 0.17Sr	0.25	6.15	1.98
Mg 1.26Ca 1.06Mn 0.30Sr	0.34	3.30	5.79
Mg 0.31Ca 0.58Mn 0.16Sr	0.22	0.00	3.10

Through a semi-automatic Rietveld refinement procedure phase percentages were also calculated using the XRD difractograms. The results are listed in table 7.

Table 7. Phase fractions (wt%) from XRD using semi-automatic Rietveld refinement

Sample	**Phase fraction (wt%)**		
Composition in wt%	**Mn**	**Mg_2Ca**	**$Mg_{17}Sr_2$**
Mg 0.45Ca 1.82Mn	0.5	0.2	-
Mg 0.21Ca 1.05Mn	0.0	0.6	-
Mg 0.17Ca 1.10Mn	0.0	3.5	-
Mg 0.52Ca 0.62Mn	0.2	5.6	-
Mg 1.49Ca 0.51Mn	0.1	4.2	-
Mg 0.51Mn 0.86Sr	0.3	-	4.9
Mg 0.64Mn 0.65Sr	0.2	-	11.3
Mg 1.27Mn 0.11Sr	0.1	-	2.2
Mg 1.86Mn 0.1Sr	0.4	-	1.6
Mg 0.73Mn 0.28Sr	0.4	-	9.0
Mg 2.21Ca 0.50Mn 0.17Sr	0.1	5.5	0.9
Mg 1.26Ca 1.06Mn 0.30Sr	0.1	6.4	1.7
Mg 0.31Ca 0.58Mn 0.16Sr	0.1	0.8	1.9

If previous studies on element solubility are taken into account (solid solubility in Mg: 2.00 wt% Mn [11], 1.34 wt% Ca, 0.11 wt% Sr [3]), the micrograph analysis data are the most accurate and reliable. Since Mn has the highest solubility in Mg out of the three

alloying elements, the majority of this element is expected to be in solid solution. Thus the experimental data coming from micrograph analyses were considered as the real ones, while theoretical calculations (from Thermo-Calc and Pandat softwares) and semi-experimental (with XRD experimental results together with Rietveld approach) were compared to those ones.

4.1.3 Mechanical properties

4.1.3.1 Hardness

To get the hardness data, several indentations were performed with the durometer in each sample. A mean value was obtained and the results with their corresponding error are ranked in the following table from hardest to softest:

Table 8. Vickers hardness (HV) ranking of the different samples

Sample	HV0.025	Error %
Mg 2.21Ca 0.50Mn 0.17Sr	56.86±3.19	5.61
Mg 1.26Ca 1.06Mn 0.3Sr	55.88±2.63	4.71
Mg 0.51Mn 0.86Sr	52.43±2.52	4.81
Mg 0.64Mn 0.65Sr	51.45±3.59	6.98
Mg 1.49Ca 0.51Mn	49.57±4.49	9.01
Mg 0.52Ca 0.62Mn	46.74±3.82	8.17
Mg 0.45Ca 1.82Mn	46.55±1.62	3.48
Mg 0.31Ca 0.58Mn 0.16Sr	46.09±4.35	9.44
Mg 0.73Mn 0.28Sr	45.65±3.99	8.74
Mg 0.21Ca 1.05Mn	44.51±5.38	12.09
Mg 1.86Mn 0.1Sr	40.53±2.53	6.24
Mg 1.27Mn 0.11Sr	39.94±4.98	12.47
Mg 0.17Ca 1.1Mn	39.31±3.83	9.74
Pure Mg	31.57±2.97	9.41
Pure Mg	30.6±5.41	17.68

From the presented results it can be inferred that the act of alloying, on its own, has a very important influence on hardness. This is due to the "solution hardening" phenomenon. Even the softest alloy composition (Mg 0.17Ca 1.1Mn) has a HV0.025 value of 39.31 improving that of pure Mg (which is HV0.025 of approximately 31) by around 25%, and the HV0.025 number of 56.86 for the hardest alloy (Mg 2.21Ca 0.50Mn 0.17Sr) is close to twice as much that of pure Mg.

Considering the existing data on human bones (Human bone hardness = 0.049-0.579 GPa = 5-59 HV [48]. Human cancellous bone hardness = 33-45 HV [49]) it can be concluded that, at least in this aspect, the alloys are more similar to bones than pure Mg. This indicates the convenience of alloying in implant applications.

The quaternary system appears to have the highest hardness. The combination of Ca and Sr produces and addition effect if they are present in a correct amount. In the case of

Mg 0.31Ca 0.58Mn 0.16Sr, the amount of alloying elements should be increased if a higher hardness is wanted.

The Mg-Mn-Sr system seems to have higher hardness compared to the other ternary, Mg-Ca-Mn, assuming the adequate minimum of alloying element is added.

These observations can also be linked to the presence of secondary phases and their strengthening effect [6]. Taking into account the numbers from table 6, the five samples with higher wt% of secondary phases are also the five ones with higher hardness, although the order varies. Hardness can thus be closely related to secondary phases. They produce a local coarsening effect, pinning dislocations, hindering deformation and impeding the advance of the indentator. These five compositions are the ones that have a defined and relatively cohesive network of secondary phases as can be appreciated on the SEM micrographs (see figures 37 a), b) and c), 39 c), e) and f) and 40 a) and b)). The other samples lack this intermetallics grid, having only isolated particles (e.g. figure 39 a) and b)), or, if it is present, it doesn't have enough cohesion to translate into significant improvement to mechanical properties (see figures 37 e) and f), 40 c), d), e) and f) and figure 41).

The grain refinement produced by alloying can also justify the obtained data in a similar way. Dislocation movement is obstructed by the higher number of grain boundaries.

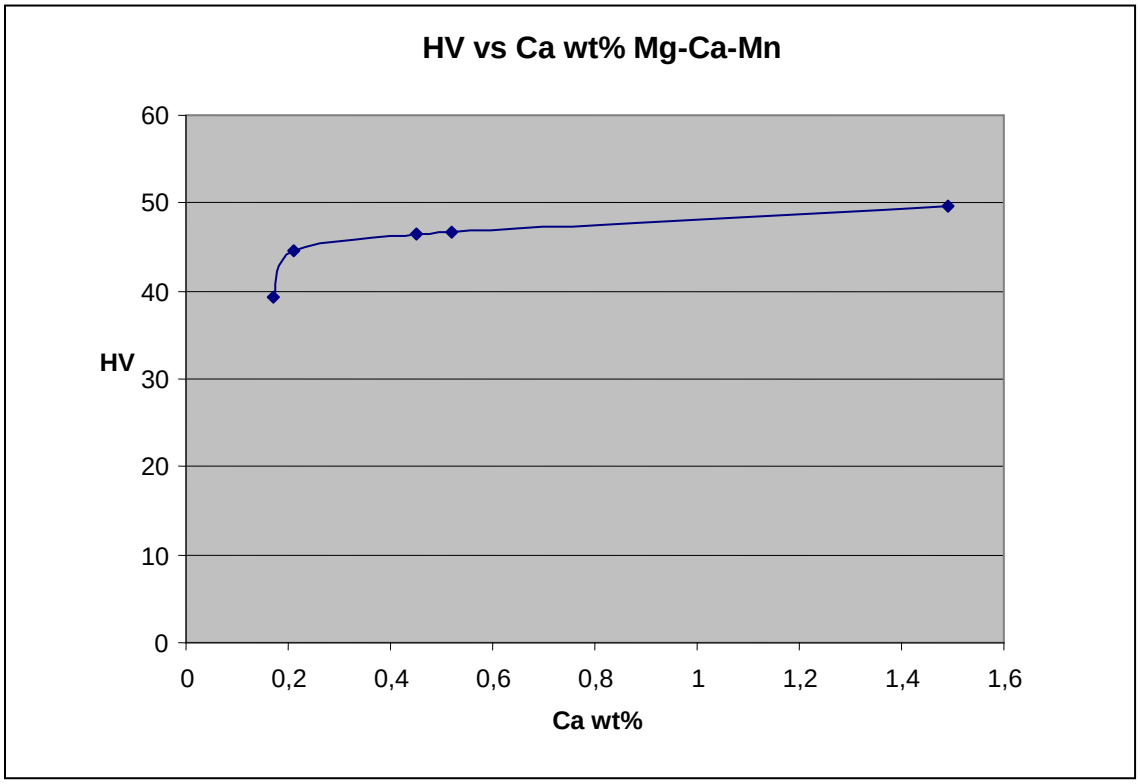

Figure 30: Hardness values (HV0.025) vs. Ca content (in wt%) for the Mg-Ca-Mn system

Since Mn does not combine with any of the other three elements, appearing only alone as a precipitate (forming small randomly situated particles) when it is present in significantly high amount and the Mg matrix is saturated, its relevance in hardening is more limited than that of Ca or Sr. Aside from the solid solution effect, saturated Mn leads to hardness decrement when it is present in higher percentages than 1 wt%. Thus,

with respect to maximization of this mechanical property, the minimum level of added Mn should be around 0.5 wt%, not exceeding 0.9 wt% (above 0.75 wt% the HV increases very little, and it doesn't improve after 0.9 wt% is reached). It must be taken into account that solubility of Mn in Mg is around 2 wt% [11].

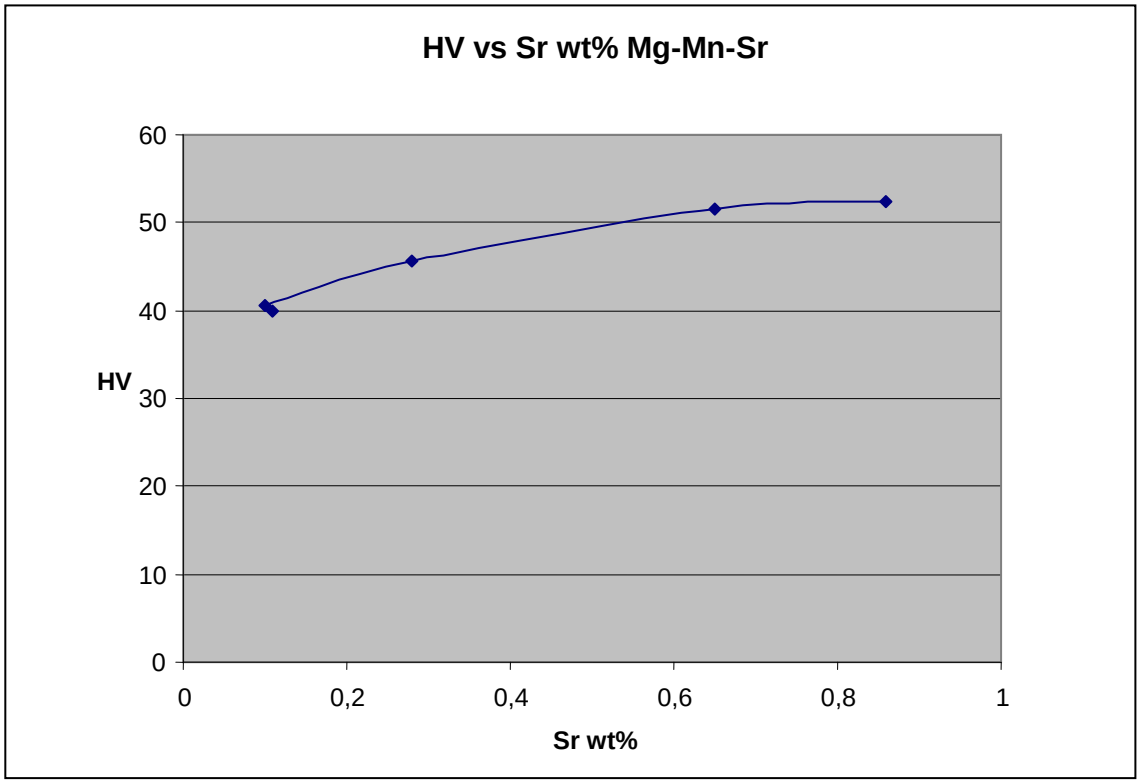

Figure 31: Hardness values (HV0.025) vs. Sr content (in wt%) for the Mg-Mn-Sr system

Considering Ca and Sr have a 1.34 wt% and 0.11 wt% solubility in Mg (respectively) [3], after saturation is achieved, further hardness increase is due to the appearance of secondary phases. The effect of Sr seems to be more important than that of Ca. Looking at figure 30, the adequate amount of added Ca is around 0.5 wt% (further increase up to 1.5 wt% produces a very low improvement). On the other hand, from figure 31 it can be concluded that the optimal amount of Sr alloying element is around 0.75 wt%.

4.1.3.2 Compressive strength

The compressive test provides various data related to mechanical behaviour and properties. Table 9 includes compressive yield strength and compression percentage (%) at ultimate compressive strength (UCS).

All alloyed samples have clearly higher compressive yield strength than pure Mg. The least stiff alloy (Mg 0.21Ca 1.05Mn) has around one third higher compressive yield strength than pure Mg, while the stiffest alloy (Mg 0.51Mn 0.86Sr) is four times stiffer. This general improvement is probably based on grain refinement and the associated solution hardening phenomenon, although secondary phases play a significant role also.

The compression % at UCS is, however, improved or worsened in comparisson to pure Mg depending on the specific alloy. Generally speaking alloying increases very little or, more usually, decreases compression % at UCS. There is a tradeoff between the two properties, with some alloys being more balanced than others. Mg 0.45Ca 1.82 Mn is the

only composition that distinctly enhances both properties. The especific application and the ensuing requirements should point out which alloy is appropriate.

Table 9. Compressive yield strength and compression % at ultimate compressive strength

Sample	Compressive yield strength at 0.2 % (MPa)	Error %	Compression % at UCS	Error %
Mg 0.45Ca 1.82Mn	49.72±1.81	3.65	37.36±2.62	7.01
Mg 0.21Ca 1.05Mn	31.96±1.53	4.79	23.18±2.71	11.68
Mg 0.17Ca 1.10Mn	34.75±0.89	2.56	29.64±0.65	2.19
Mg 0.52Ca 0.62Mn	50.53±2.14	4.23	26.25±1.52	5.81
Mg 1.49Ca 0.51Mn	80.77±2.15	2.66	20.91±4.87	23.3
Mg 0.51Mn 0.86Sr	97.22±5.23	5.38	14.72±1.88	12.81
Mg 0.64Mn 0.65Sr	86.83±8.73	10.06	13.51±0.50	3.68
Mg 1.27Mn 0.11Sr	49.23±1.08	2.19	32.15±2.52	7.85
Mg 1.86Mn 0.1Sr	54.16±1.61	2.97	32.43±1.60	4.93
Mg 0.73Mn 0.28Sr	62.16±1.04	1.67	18.52±2.44	13.18
Mg 2.21Ca 0.5Mn 0.17Sr	93.98±1.16	1.24	18.24±2.54	13.94
Mg 1.26Ca 1.06Mn 0.3Sr	80.77±1.86	2.31	25.46±1.96	7.7
Mg 0.31Ca 0.58Mn 0.16Sr	58.70±1.21	2.06	29.46±2.54	8.64
Pure Mg	24.69±1.79	7.26	34.42±1.90	5.51
Pure Mg	23.69±1.24	5.25	33.29±2.80	8.42

The engineering compression stress vs. engineering strain curves are represented in figures 32 to 35, sorted by system. The differences in mechanical properties such as compressive yield strength and UCS amongst the varying compositions can be percieved.

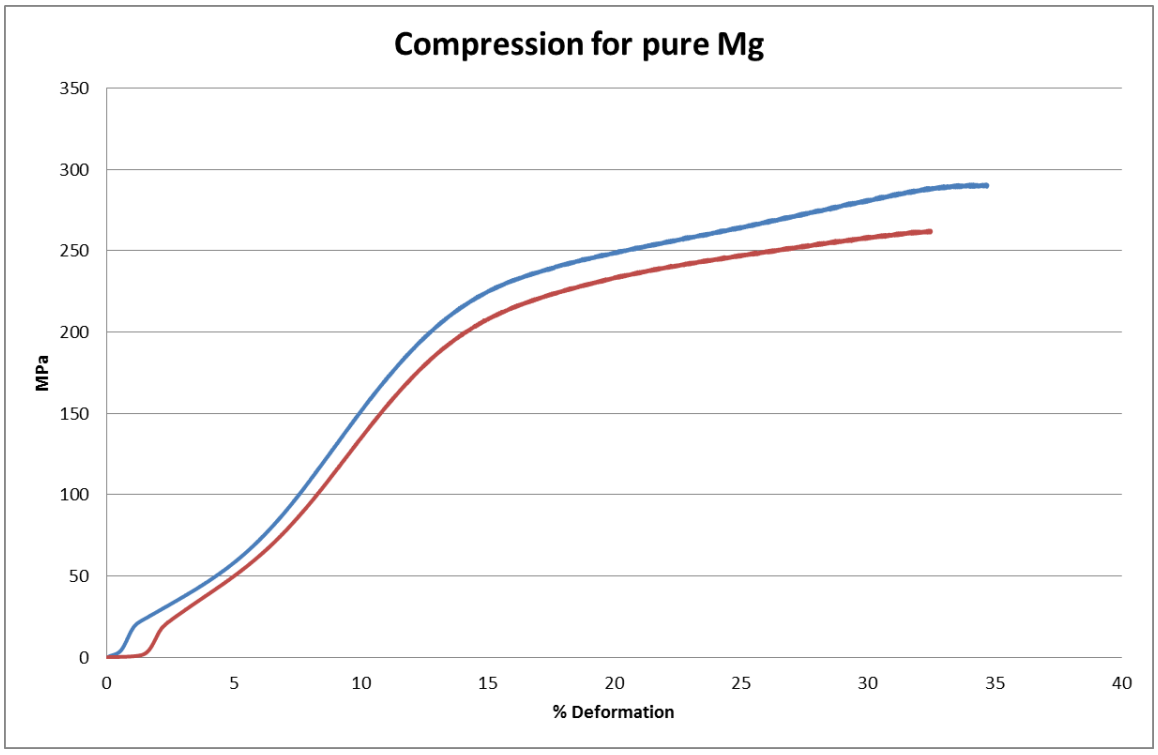

Figure 32: Engineering compressive stress vs. engineering strain curves for pure Mg

Note: In the case of pure Mg, of which two gravity cast rods were manufactured, two different batches of compression specimens were obtained, one for each cast rod, so two different sets of compression tests were done, one for each cast rod. Hence the two curves.

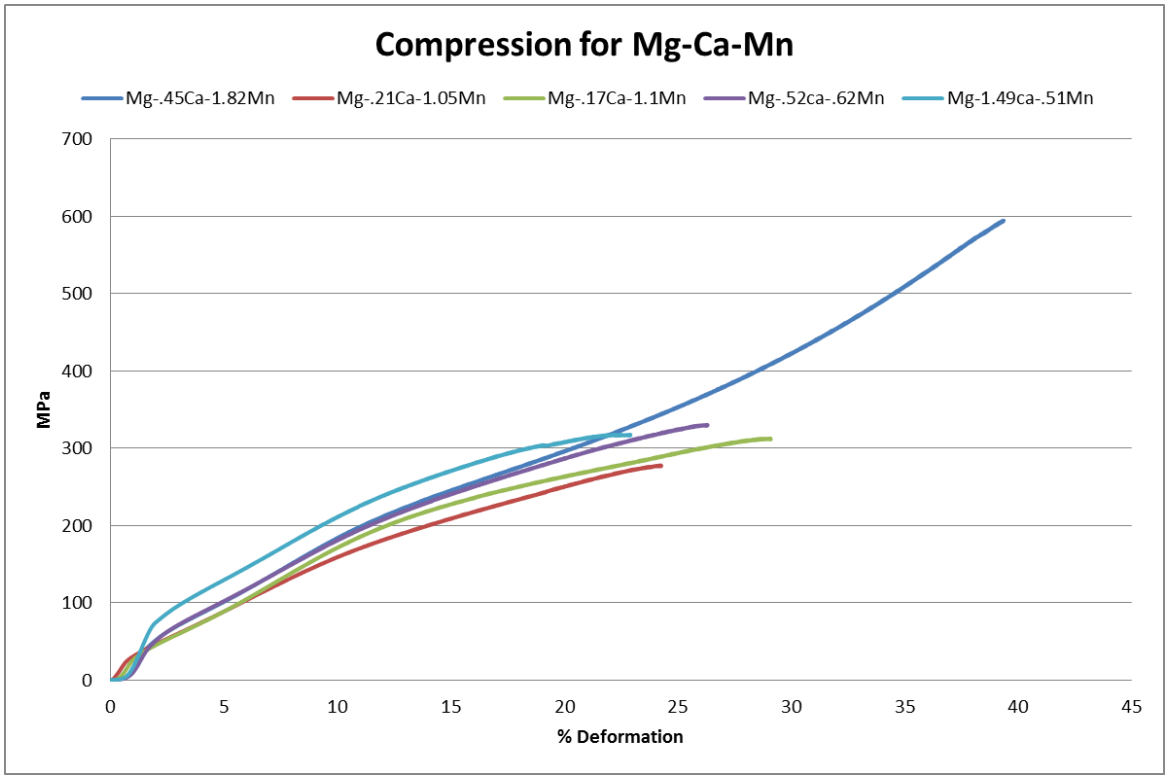

Figure 33: Engineering compressive stress vs. engineering strain curves for Mg-Ca-Mn

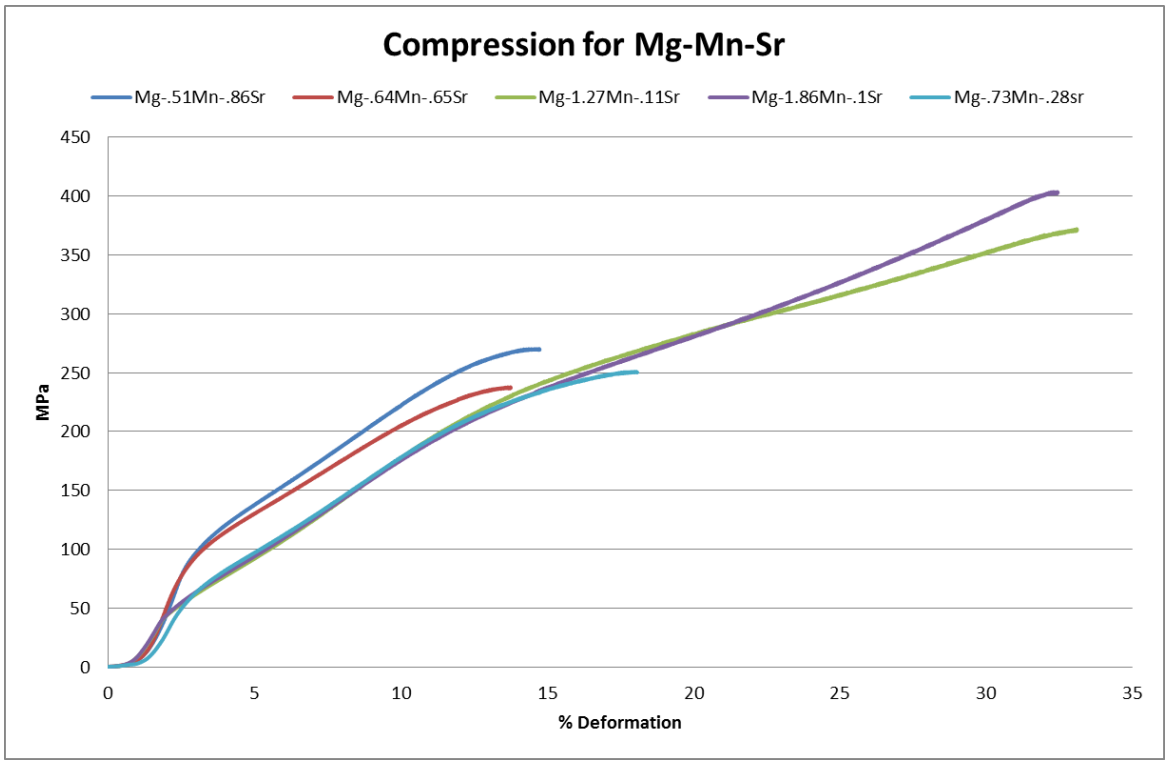

Figure 34: Engineering compressive stress vs. engineering strain curves for Mg-Mn-Sr

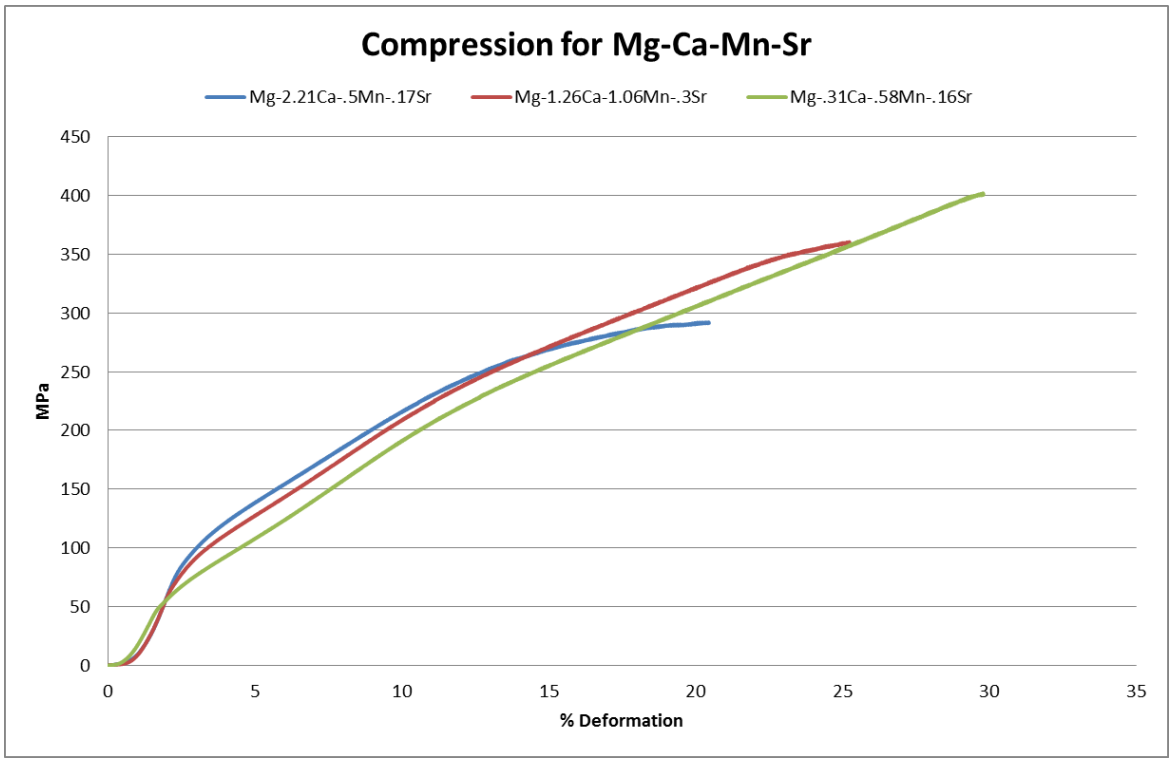

Figure 35: Engineering compressive stress vs. engineering strain curves for Mg-Ca-Mn-Sr

A change in the slope at the beginning of the curves can be appreciated in the figures. This is characteristic of the hexagonal structure (Mg has a hexagonal close packed (HCP) structure), in which deformation depends on the initial texture of the sample. In this case, the as cast samples have no texture, crystals are randomly oriented. There are two main deformation mechanisms in Mg at room temperature, basal slip and twinning. In the tested samples, twinning takes place at the beginning of deformation. This produces reorientation via rotation of basal planes (i.e. base of the hexagonal prism that constitutes the unit cell), creating a basal fibre texture. Basal slip ensues [21,26,50].

The three different systems can be analysed individually or all together, extracting several observations.

Focusing on figure 33, the curves look quite similar exceptuating the compression % at UCS of Mg 0.45Ca 1.82Mn and the compressive yield strength of Mg 1.49Ca 0.51Mn. The first "anomaly" can be explained with the high Mn content of that composition. As stated in previous studies, Mn seems to enhance ductility (or, more precisely, keep it close to pure Mg levels) [11,26]. The other significant variation can be linked to the eutectic phase network containing the intermetallic Mg_2Ca that forms in Mg1.49Ca 0.51Mn (see figure 39 c)). This Laves type phase has the ability to pin grain boundaries, improving rigidity [51].

The curves for the Mg-Mn-Sr system in figure 34 show the significant variations that relatively minute changes in Sr content produce. Compressive yield strength and compression % at UCS are directly and inversely dependant on Sr content, respectively. Again, high amounts of Mn increase ductility. Thus, the mechanical porperties of this system should be easy to tailor, since Mn promotes ductility and Sr stiffness. Depending on the requirements, the desired properties could be achieved with a certain content of

Mn and Sr. A whole range of strengths can be attained by slight variations of the percentage of alloying elements. However, if ductility is not to be compromised and Mn content needs to be kept low, Sr should be below 0.2 wt%.

The samples for the quaternary Mg-Ca-Mn-Sr system, with the corresponding engineering compressive stress vs. strain curves depicted in figure 35, clearly confirm a relatively general rule: The more alloyed the lower ductility and the higher yield strength. The defined and cohesive intermetallic phases grid that forms in Mg 2.21Ca 0.5Mn 0.17Sr and Mg 1.26Ca 1.06Mn 0.3Sr, notably with the presence of eutectic Mg_2Ca (more in Mg 2.21Ca 0.5Mn 0.17Sr than Mg 1.26Ca 1.06Mn 0.3Sr and outright absent in Mg 0.31Ca 0.58Mn 0.16Sr), increases compressive yield strength thanks to the grain boundary pinning effect [51]. However, it should be taken into account that this increased mechanical performance could go together with deterioration of other properties. For instance, if the intermetallics network is too continuous, too interconnected, corrosion resistance could decrease [52]. Furthermore, there is a limit in intermetallic phase content that should not be surpassed. A very thick and interlinked network can lead to a general performance decline, including mechanical.

The previously mentioned ductility enhancement effect of relatively high amounts of Mn seems to occur above 1.1 wt% Mn. If the aim is to obtain high ductility, Mn content should be in the 1.5-2 wt% range.

4.2 Mechanical alloyed and SPS manufactured

The powder metallurgy (PM) approach to biomedical parts manufacturing offers several advantages. In comparison with gravity casting, the material loss during processing is much lower, minimal. There is no need to add a higher amount of a certain alloying element to compensate its loss due to evaporation or oxidation. Such a risk does not exist in PM because the manufacturing temperature is below the melting point of the materials. Segregation phenomena are also greatly attenuated. The lower operating temperature also translates in energy, cost and time savings. As stated before, the potential issue of porosity brought by PM can turn into an advantage in bioengineering applications, providing sites for drug introduction before implant surgery and for cells to grow [27]. Also, porosity means lower density, hence closer to that of bone.

Whereas the casting process usually needs to be followed by one or various secondary processes, such as a heat treatment to get rid of the typical ingot crystalline structure or rolling to improve mechanical properties, the parts manufactured with Spark Plasma Sintering (SPS) do not have this issue. This PM method is especially recommended for small orthopedic implant parts, such as pins and rods (and also more complex pieces). Using the adequate mould, the parts manufactured via SPS can be considered finished products (or needing minor finishing processes), since the low temperatures not only permit high precision in composition but also in shape and size. Furthermore, the drug bearing and osseointegration possibilities that porosity provides mean that the surface obtained after SPS can be the desired one, needing little or no surface finishing processes [27].

Comparing SPS to other PM processes, the main advantages of the former are: Lower temperature (Joule heating plays an important role), lower process time (higher heating/cooling rates, internal vs. external heating), higher densification, better mechanical properties (chiefly due to no significant grain growth in SPS compared to other PM methods) [41], elimination of oxides (thanks to the pulses), better quality (decreasing need of finishing processes).

To produce a high quality raw material for the SPS process, mechanical alloying was performed. After trying several configurations, the optimal setting was found to be the following: 30-35:1 ball to powder milling ratio, 900 rpm, 18h milling time.

The optimal ball to powder milling ratio was reached after trying various setups. The approach to the tuning of this process parameter was to try to keep the ratio as low as possible (i.e. less balls and more material) to fit the largest amount of material possible into the vessel, thus maximizing powder production. Ratios as low as 10:1 were used, but with that configuration milling simply does not occur, the material experiences no significant change. There is a minimum critical amount and ratio of milling media needed for particle size reduction to happen. Milling balls have to occupy at least 30-40% of the zirconia vessel volume capacity.

A higher milling time does little in improving the powder quality. On the other hand, increasing time does result in higher risks of material sticking to the milling media and vessel, as previously explained. This issue is more important in this case because Mg is relatively soft, hence the need to use lubricant. It is worth noting that stearic acid was used as lubricant because it evaporates easily in the following process with the first SPS pulses, so getting rid of it is fairly simple.

Milling times of up to 20 or even 25 hours were used. The powder quality and its size distribution, which typically follows a Gaussian function pattern (i.e. a powder will be composed of a whole range of different sized particles, with higher or lower homogeneity depending on the quality), were enhanced in relation with increasing time up to approximately 18-20 hours of milling. Beyond that, however, more mechanical alloying time did not show further significant improvement.

Cryomilling was somewhat a failure mainly due to technologic constraints. No further cooling could be provided during the milling step, so proper cryomilling was probably not achieved, no difference could be appreciated.

The SPS conditions previously mentioned were set taking into account existing publications [27,39-43] and the nature of the elements in question. Mg is the main component and has the lowest melting point at 650°C [1]. Considering this the sintering temperature was set at 500°C. A higher temperature would be too close to the 650°C mark. A 20MPa pressure was applied. In order to avoid pernicious flow stress phenomena, increasing pressure and temperature above these levels should be done with care. The used settings are thus considered safely optimal.

4.2.1 Powder analysis

Ocular inspection of the mechanically alloyed powders is very helpful in quickly determining the success of the procedure. In the first trials, 3.35 mm diameter Ca

granules were used as source for that element. Upon visual analysis of the milled material it became apparent that a significant and unacceptably high amount of Ca granules did not break down. Consequently the Ca source was changed to Mg10Ca master alloy turnings, with greater success.

The powders were analysed using SEM microscopy to determine homogeneity, quality and size. The 18h milled powder was deemed to be the best one. It has an angular shape (typical of the mechanical process of obtention), with a size of around 10 µm and significant homogeneity. On the other hand, powders milled during a shorter period are larger and less homogeneus. Figure 36 depicts SEM micrographs that can serve as illustration of the varying nature of the powders.

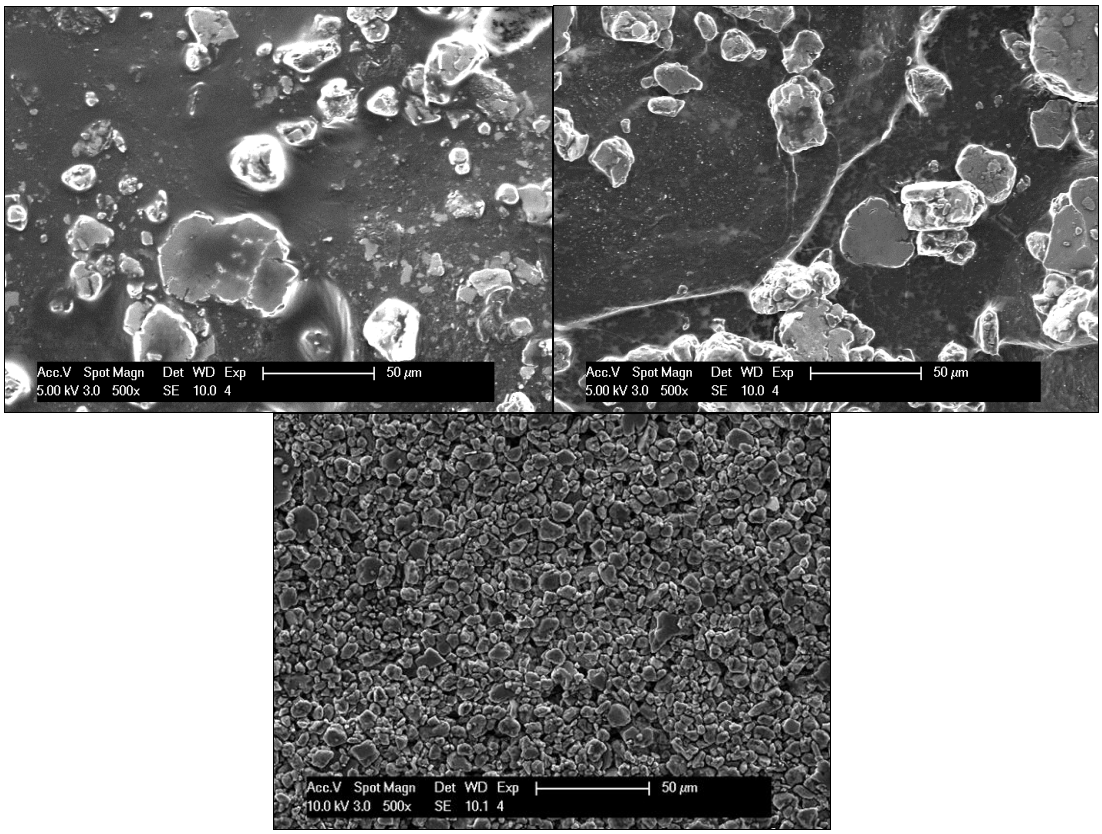

Figure 36: SEM micrographs of powder after 6h (left), 13h (right) and 18h mechanical alloying

After SPS manufacturing of the mechanically alloyed powders the resulting samples were also analysed, with optical and SEM microscopes. The obtained cylinders were cut to obtain two half cylinders. The inner surface that originates was ground, polished (the sample preparation procedure previously explained was followed) and analysed. A refinement of the microstructure was observed with increasing milling time up to 18h (see figures 45 and 46 in appendix).

4.2.2 Density and porosity

To address the quality of the SPS manufactured discs, density was measured following the Archimedes method. The following table shows the results ranked from

most to least densified of the SPS samples from the Mg-Ca-Mn system, with similar compositions to the five cast samples from the same ternary system introduced in previous sections of this thesis (Other samples were manufactured and they can be found on table 13 in appendix):

Table 10. Density and densification ranking of the SPS samples obtained using the Archimedes measurement kit

Sample	Density (g/cm^3)	Error %	Densification %
Mg 1.49Ca 0.51Mn	1.7339±0.0005	0.03	99.89
Mg 0.45Ca 1.82Mn	1.7542±0.0005	0.03	98.46
Mg 0.52Ca 0.62Mn	1.6173±0.0007	0.04	93.16
25h Mg 0.21Ca 1.05Mn	1.526±0.003	0.21	87.22
Mg 0.17Ca 1.1Mn	1.53±0.03	1.76	87.12
Mg 0.21Ca 1.05Mn	1.46±0.02	1.70	83.51

Note: All samples were mechanically alloyed for 20h except for one of the Mg 0.21Ca 1.05Mn samples that was milled for 25h.

Utilizing isothermal calculations a prediction of the phase fractions at the sintering temperature of 500°C can be performed. With these phase fractions an estimate of density can be done. The results can be observed on tables 11 and 12. Using the two predictions an average density was obtained for each composition, with which the densification % was calculated.

Table 11. Phase fractions (wt%) from Thermo-Calc (TCMG2 database) at 500°C and sample densities

Sample	Phase fraction (wt%)		Density (g/cm^3)
Composition in wt%	Mn	Mg_2Ca	
Mg 0.45Ca 1.82Mn	1.10	0.00	1.79912
Mg 0.21Ca 1.05Mn	0.32	0.00	1.75436
Mg 0.17Ca 1.10Mn	0.37	0.00	1.75723
Mg 0.52Ca 0.62Mn	0.00	0.00	1.736
Mg 1.49Ca 0.51Mn	0.00	1.97	1.73559

Table 12. Phase fractions (wt%) from Pandat (Mg-Ca-Mn database) at 500°C and sample densities

Sample	Phase fraction (wt%)		Density (g/cm^3)
Composition in wt%	Mn	Mg_2Ca	
Mg 0.45Ca 1.82Mn	0.49	0.00	1.76412
Mg 0.21Ca 1.05Mn	0.14	0.00	1.74403
Mg 0.17Ca 1.10Mn	0.16	0.00	1.74518
Mg 0.52Ca 0.62Mn	0.00	0.00	1.736
Mg 1.49Ca 0.51Mn	0.00	1.63	1.73566

From these data it can be inferred that some samples densified successfully while others did not. Amongst those where “full density” was not achieved, some had

significant porosity. The process can thus produce acceptable results, but there could be a consistency issue. The presence of alloying elements and particularly Ca seems to enhance densification, supporting previous studies that show beneficial effects of Ca in sintering (through protection against oxidation and directly promoting the sintering phenomenon via diffusion of Ca into Mg) [27], while the effect of Mn could be less important. Although it appears promising, further investigation into this manufacturing method is definitely needed.

Chapter 5

Conclusions & future work

5.1 Conclusions

The gravity cast samples of the Mg-Ca-Mn, Mg-Sr-Mn and Mg-Ca-Mn-Sr systems were characterised, acquiring information about their composition, microstructure and mechanical behaviour. These mechanical properties were successfully linked to variation of alloying content, grain size and nature and percentage of secondary phases.

Preliminary thermodynamic calculations were found to be accurate and helpful in deciding what compositions to use to produce samples containing the desired beneficial intermetallics. In general terms, the phases predicted to be present where found in the manufactured samples. No other unexpected phases were found. The thermodynamically calculated phase percentages did not exactly match the SEM micrographs and Rietveld refinement analyses, but they are deemed a good initial estimation for the material design process.

Thanks to the so called third element effect (by which the presence of a third element diminishes the threshold content of other elements needed to significantly improve the material properties) the percentage of alloying elements could be kept low while still getting a final product with significantly enhanced properties.

There appears to be a need to have enough alloying content to promote formation of interconnected secondary phases. This network of intermetallic compounds serves as grain boundary sliding hindrance and dislocation pinner, effectively improving

mechanical behaviour. The intermetallics grid provides a notable quality leap in mechanical properties. Consequently, Mg 1.49Ca 0.51Mn in the Mg-Ca-Mn system, Mg 0.51Mn 0.86Sr and Mg 0.64Mn 0.65Sr in the Mg-Mn-Sr system and Mg 2.21Ca 0.50Mn 0.17Sr and Mg 1.26Ca 1.06Mn 0.3Sr in the Mg-Ca-Mn-Sr system showed significant performance.

Nevertheless, looking at the bigger picture, it is worth noting that, aside from good mechanical behaviour, corrosion resistance is also very important for the intended applications. If the intermetallic network is too thick and interconnected it could accelerate degradation.

A safe compromise could then be to heed the following recommendations for alloying contents: 0.5 wt% Ca, 0.75 wt% Sr and 0.5 wt% Mn. These suggested levels are in the minimal side, meaning that relatively higher percentages can be used, but lower ones are not advised. It must be also noted that there are many factors that could change these suggestions, such as the number of different elements in the alloy, the manufacturing method, the specific application, etc. Furthermore, when considering bone implants, variables like patient age or the part of the body where it is located matter greatly.

From the experience of this work, the mechanical alloying together with SPS as processing route is viable and highly recommended, at least in the case of the Mg-Ca-Mn system.

The mechanical alloying setting (optimized to: 30-35:1 ball to powder milling ratio, 900 rpm, 18h milling time) produced powders of satisfactory quality for the following SPS manufacturing step. With the SPS setting (i.e. initial heating up to 450°C followed by controlled heating rate of 10°C/min up to 500°C, then sintering during five minutes at 500°C and 20 MPa), varying degrees of densification, up to virtual full density, were attained. Ca seems to play an important role in densification, more so than Mn. The manufactured parts could serve biomedical applications very well, especially in the case of bone implants due to the potential advantages of porosity.

5.2 Future work

A study of more Mg-Mn-Sr system compositions, to tailor and reach ideal mechanical properties (ductility vs. stiffness, Mn promotes the former, Sr the later), is suggested.

Comprehensive identification of Mg-Ca-Sr phases is recommended in the Mg-Ca-Mn-Sr quaternary system. For this Transmission Electron Microscopy (TEM) would be appropriate since the description of the system is still not available in the literature.

Corrosion experiments and further biomedical studies are needed to determine the viability of the manufactured samples. In vitro and in vivo tests are being carried out within the MagnIM project [53].

The recommendation of mechanical alloying followed by SPS could probably be extended to other systems (e.g. Mg-Mn-Sr and Mg-Ca-Mn-Sr), but in order to assure this statement more studies and experiments are needed.

On the other hand, work is still to be done to solve SPS inconsistency issues, especially if large scale production is sought. Oxidation could be to blame for this, although an Ar atmosphere was used during the PM manufacturing process. Further analysis of the many factors involved in the process is required.

In the mechanical alloying manufacturing step, proper cryomilling could be significantly helpful. For this, continuous cooling during the process would be needed; a suitable cooling system is suggested to get better results (like finer powder in shorter time, thanks to the embrittlement effect). It would have an influence mainly by decreasing milling time and avoiding cold welding. Monitoring temperature inside the milling vessels could also aid in this task (and in improving the process in general, to have more control over it, determining how temperature evolves, when it stabilizes, etc.). Another potential improvement to this procedure could be the introduction of short breaks (e.g. stopping the machine during 20-30 minutes once or twice).

References

[1] H.E. Boyer, T.L. Gall, Metals handbook, Desk edition, American Society for Metals, Metals park, Ohio 44073, ISBN 0-87170-188-X (1985)

[2] M.P. Staiger, A.M. Pietak, J. Huadmai, G. Dias, Magnesium and its alloys as orthopedic biomaterials: A review, Biomaterials 27:1728-1734 (2006)

[3] Y.F. Zheng, X.N. Gu, F. Witte, Biodegradable metals, Materials Science and Engineering R 77:1-34 (2014)

[4] H.R. Bakhsheshi-Rad, M.H. Idris, M.R. Abdul-Kadir, A. Ourdjini, M. Medraj, M. Daroonparvar, E. Hamzah, Mechanical and bio-corrosion properties of quaternary Mg-Ca-Mn-Zn alloys compared with binary Mg-Ca alloys, Materials and Design 53:283-292 (2014)

[5] S.S Abd El-Rahman, Neuropathology of aluminum toxicity in rats (glutamate and GABA impairment), Pharmacological Research 47:189-194 (2003)

[6] M. Bornapour, M. Celikina, M. Cerruti, M. Pekguleryuz, Magnesium implant alloy with low levels of strontium and calcium: The third element effect and phase selection improve bio-corrosion resistance and mechanical performance, Materials Science and Engineering C 35:267-282 (2014)

[7] T.D. Luckey, B. Venugopal, Metal toxicity in mammals, Plenum Press, New York, 167-168 (1977)

[8] R.V. Suganthi, K. Elayaraja, M.I.A. Joshy, V.S. Chandra, E.K. Girija, S.N. Kalkura, Fibrous growth of strontium substituted hydroxyapatite and its drug release, Material Science & Engineering C, Materials for Biological Applications 31:593-599 (2011)

[9] W.B. Zhang, Y.H. Shen, H.B. Pan, K.L. Lin, X.G. Liu, B.W. Darvell, W.W. Lu, J.A. Chang, L.F. Deng, D.P. Wang, W.H. Huang, Effects of strontium in modified biomaterials, Acta Biomaterialia 7:800-808 (2011)

[10] S.E. Harandi, M.H. Idris, H. Jafari, Effect of forging process on microstructure, mechanical and corrosion properties of biodegradable Mg-1Ca alloy, Materials & Design 32:2596-2603 (2011)

[11] H.E. Friedrich, B.L. Mordike, Magnesium Technology-Metallurgy, Design Data, Applications, Berlin, Heidelberg: Springer-Verlag (2006)

[12] N. Hort, Y. Huang, K. U. Kainer, Intermetallics in magnesium alloys, Advanced Engineering Materials 8 Nº4:235-240 (2006)

[13] http://www.magnim.eu/index.php?id=17 (Last accessed on 26/10/15)

[14] L. Cheah, C. Evans, A. Bandivadekar, J. Heywood, Factor of two: Halving the fuel consumption of new U.S. automobiles by 2035, Laboratory for Energy and the Environment, Report Nº LFEE 2007-04 RP, Massachusetts Institute of Technology (2007)

[15] M. Pacchione, J. Telgkamp, Challenges of the metallic fuselage, 25th Congress of International Council of the Aeronautical Sciences, Paper ICAS 2006-4.5.1 (2006)

[16] H. Watarai, Trend of research and development for magnesium alloys, Science & Technology Trends 18:84-97 (2006)

[17] A.B. Novaes Jr., S.L. Scombatti de Souza, R.R. Martins de Barros, K.K. Yamashina Pereira, G. Iezzi, A. Piattelli, Influence of implant surfaces on osseointegration, Braz Dent J 21(6):471-481 (2010)

[18] F. Witte, The history of biodegradable magnesium implants: A review, Acta Biomaterialia 6:1680-1692 (2010)

[19] M. Niinomi, Recent metallic materials for biomedical applications, Metallurgical and Materials Transactions 33A:477-486 (2002)

[20] B.L. Mordike, T. Ebert, Magnesium properties — applications — potential, Materials Science and Engineering A 302:37-45 (2001)

[21] A.M. Fernández-Blanco, Master thesis, Evolución de la textura cristalográfica durante la deformación uniaxial de una chapa laminada de la aleación de magnesio AZ31B (2010)

[22] F. Feyerabend, J. Fischer, J. Holtz, F. Witte, R. Willumeit, H. Drückere, C. Vogte, N. Hort, Evaluation of short-term effects of rare earth and other elements used in magnesium alloys on primary cells and cell lines, Acta Biomaterialia 6:1834-1842 (2010)

[23] S.A. Khan, Y. Miyashita, Y. Mutoh, Z.B. Sajuri, Influence of Mn content on mechanical properties and fatigue behavior of extruded Mg alloys, Materials Science and Engineering A 420:315-321 (2006)

[24] Y. Ding, C. Wen, P. Hodgson, Y. Li, Effects of alloying elements on the corrosion behavior and biocompatibility of biodegradable magnesium alloys: a review, J. Mater. Chem. B 2:1912-1933 (2014)

[25] E. Zhang, D. Yin, L. Xu, L. Yang, K. Yang, Microstructure, mechanical and corrosion properties and biocompatibility of Mg-Zn-Mn alloys for biomedical application. Mater Sci Eng C 29:987-93 (2009)

[26] N.V. Dudamell-Caballero, Comportamiento mecánico a alta velocidad de deformación de aleaciones de magnesio (2010)

[27] M. Wolff, T. Ebel, M. Dahms, Sintering of magnesium, Advanced Engineering Materials 12 Nº9:829-836 (2010)

[28] Patent: M.V. Manuel, H.S. Brar, I.S. Berglund, B.G. Keselowsky, M. Sarntinoranont, Bioresorbable metal alloy and implants made of same, US 13/808,037 (2014)

[29] B.J. Luthringer, F. Feyerabend, R. Willumeit-Römer, Magnesium-based implants: a mini-review, Magnesium Research 27 (4):142-54 (2014)

[30] M. Hillert, Partial Gibbs energies from Redlich-Kister polynomials, Thermochimia Acta, 129:71-75 (1988)

[31] D.L. Bish, S.A. Howard, Quantitative phase analysis using the Rietveld method, Journal of Applied Crystallography 21:86-91 (1988)

[32] Standard test methods of compression testing of metallic materials at room temperature, Designation E9-89a (Reapproved 2000), ASTM International

[33] A. Yamazaki, J. Kaneko, M. Sugamata, Mechanical alloying of Mg-Al alloy with addition of metal silicides, Materials Transactions, Vol. 45, Nº7:2410-2416 (2004)

[34] F.C. Gennari, G. Urretavizcaya, Mechanical alloying of Mg-Ge based mixtures under hydrogen and argon atmospheres, Latin American Applied Research 32:275-280 (2002)

[35] L. Dias, B. Trindade, C. Coelho, F.H. Froes, Mechanical alloying of Mg-Ti-Si light alloys and subsequent consolidation, Materials Technology (2003)

[36] A. Kumar Chaubey, S. Scudino, M. Samadi Khoshkhoo, K.G. Prashanth, N. Krishna Mukhopadhyay, B. Kanta Mishra, J. Eckert, Synthesis and characterization of nanocrystalline Mg-7.4%Al powders produced by mechanical alloying, Metals 3:58-68 (2013)

[37] G. Liang, R. Schulz, Synthesis of Mg-Ti alloy by mechanical alloying, Journal of Materials Science 38:1179-1184 (2003)

[38] J. Gubicza, M. Kassem, T. Ungár, The microstructure of mechanically alloyed nanocrystalline aluminium-magnesium, Materials Science Forum 443-444:103-106 (2004)

[39] F.O. Méar, G. Xie, D.V. Louzguine-Luzgin, A. Inoue, Spark Plasma Sintering of Mg-based amorphous ball-milled powders, Materials Transactions 50 Nº3:588-591 (2009)

[40] G. Xie, O. Ohashi, T. Sato, N. Yamaguchi, M. Song, K. Mitsuishi, K. Furuya, Effect of Mg on the sintering of Al-Mg alloy powders by pulse electric-current sintering process, Materials Transactions 45 Nº3: 904-909 (2004)

[41] W.N.A.W. Muhammad, Y. Mutoh, Y. Miyashita, Microstructure and mechanical properties of magnesium prepared by Spark Plasma Sintering, Advanced Materials Research 129-131:764-768 (2010)

[42] W.N.A.W. Muhammad, Z. Sajuri, Y. Mutoh, Y. Miyashita, Microstructure and mechanical properties of magnesium composites prepared by Spark Plasma Sintering technology, Journal of Alloys and Compounds 509 20:6021-6029 (2011)

[43] M. Wolff, C. Blawert, M. Dahms, T. Ebel, Properties of sintered Mg alloys for biomedical applications, Materials Science Forum 690:491-494 (2011)

[44]https://www.mtm.kuleuven.be/equipment/spark_plasma_sintering/spark_plasma_sintering (Last accessed on 26/10/15)

[45] Sartorius AG, User manual density determination kit, Goettingen, Germany (2008)

[46] D.H. St. John, Q. Ma, M.A. Easton, P. Cao, Grain Refinement of Magnesium Alloys, Metallurgical Materials Transactions A 36:1669-1679 (2005)

[47] Y.C. Lee, A.K. Dahle, D.H. St. John, The role of solute in grain refinement of magnesium, Metallurgical and Materials Transactions 31:2895-2906 (2000)

[48] J.K. Weaver, The microscopic hardness of bone, Journal of Bone and Joint Surgery A 48:273-288 (1966)

[49] E. Dall'Ara, C. Öhman, M. Baleani, M. Viceconti, The effect of tissue condition and applied load on Vickers Hardness of human trabecular bone, Journal of Biomechanics 40 14: 3267-70 (2007)

[50] N. V. Dudamell, I. Ulacia, F. Gálvez, S. Yi, J. Bohlen, D. Letzig, I. Hurtado, M.T. Pérez-Prado, Twinning and grain subdivision during dynamic deformation of a Mg AZ31 sheet alloy at room temperature, Acta Materialia 59:6949-6962 (2011)

[51] F. Witte, N. Hort, C. Vogt, S. Cohen, K.U. Kainer, R. Willumeit, F. Feyerabend, Degradable biomaterials based on magnesium corrosion, Current Opinion in Solid State and Materials Science 12:63-72 (2008)

[52] C. Du, Master thesis, Microstructure and properties of Mg-Zn-Mn-Ca alloys for biomedical applications (2012)

[53] http://www.magnim.eu/index.php?id=about-us (Last accessed on 26/10/15)

Appendices

Table 13. Density ranking of the SPS discs obtained using the Archimedes measurement kit

Sample	Density (g/cm^3)	Error %
13h Mg 1.5Ca 0.5Mn	1.7767±0.0004	0.02
Mg 0.45Ca 1.82Mn	1.754±0.002	0.13
Mg10Ca + Mn	1.7468±0.0008	0.05
Mg 1.49Ca 0.51Mn	1.7339±0.0005	0.03
1h Mg 1.5Ca 0.5Mn	1.7232±0.0005	0.03
Mg 1.34Ca 0.41Si	1.683±0.004	0.22
6h Mg 1.5Ca 0.5Mn	1.676±0.0003	0.02
Mg 2.8Ca 0.44Mn	1.658±0.004	0.22
Mg 0.52Ca 0.62Mn	1.6173±0.0007	0.04
Mg 0.34Ca 1.74Mn	1.611±0.004	0.23
Mg 0.27Ca 0.9Mn	1.594±0.003	0.21
Mg 0.17Ca 1.1Mn	1.53±0.03	1.76
25h Mg 0.21Ca 1.05Mn	1.526±0.003	0.21
Mg 0.21Ca 1.05Mn	1.46±0.02	1.70

Note: All samples were mechanically alloyed for 20h except those where a different time is indicated and the Mg10Ca+Mn which was not milled at all (this sample was made out of a by-product mix of Mg10Ca and Mn chips and its composition has not been precised with an analytical method).

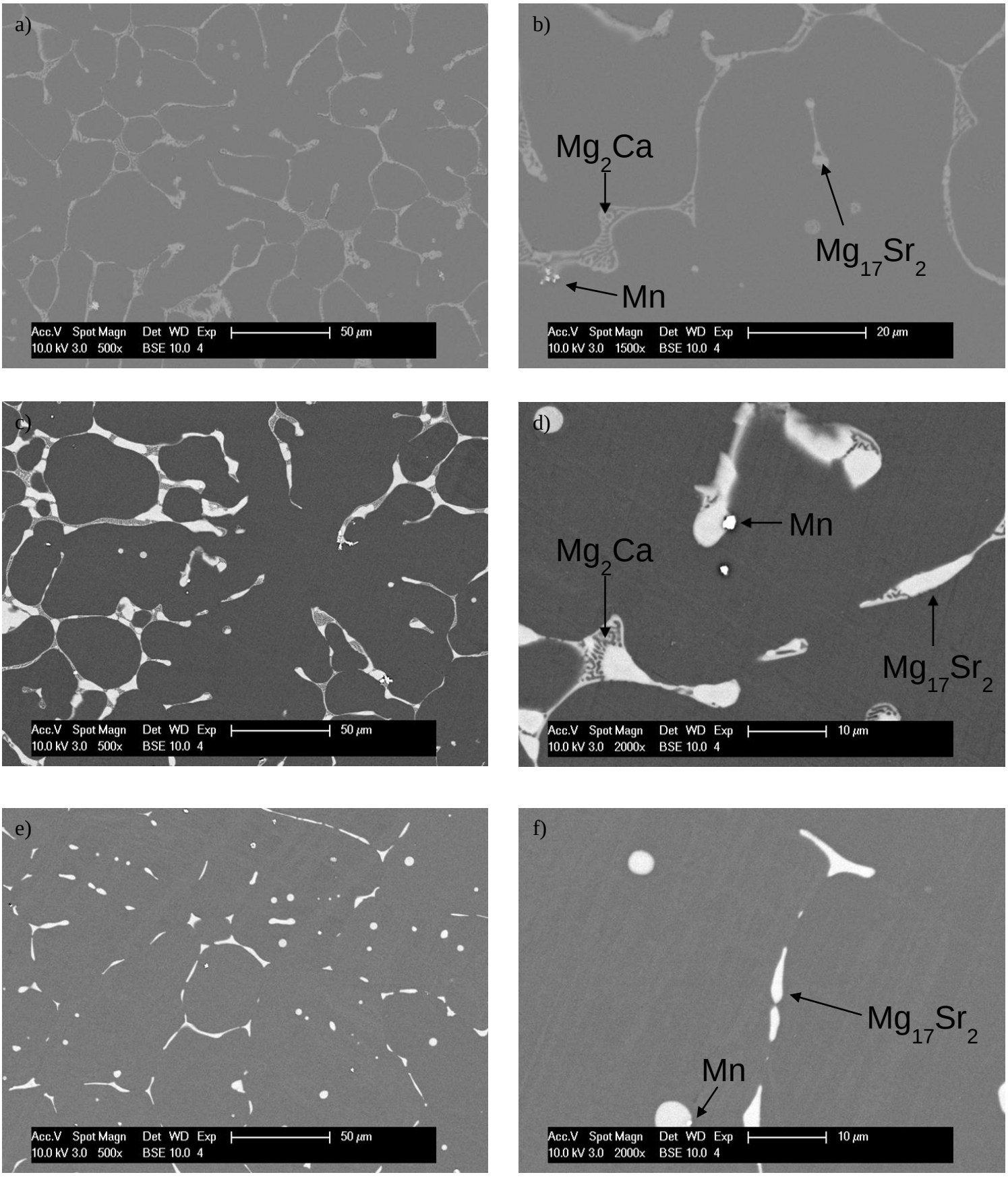

Figure 37: SEM images of a) and b) Mg 2.21Ca 0.50Mn 0.17Sr;
c) and d) Mg 1.26Ca 1.06Mn 0.30Sr; e) and f) Mg 0.31Ca 0.58Mn 0.16Sr

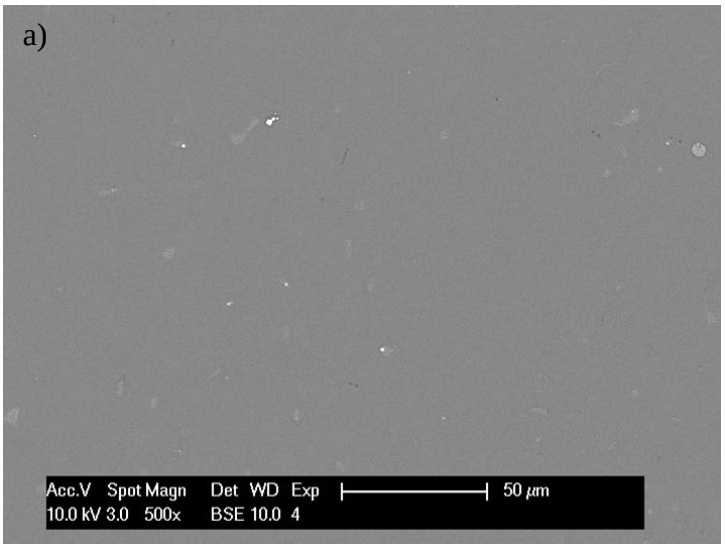

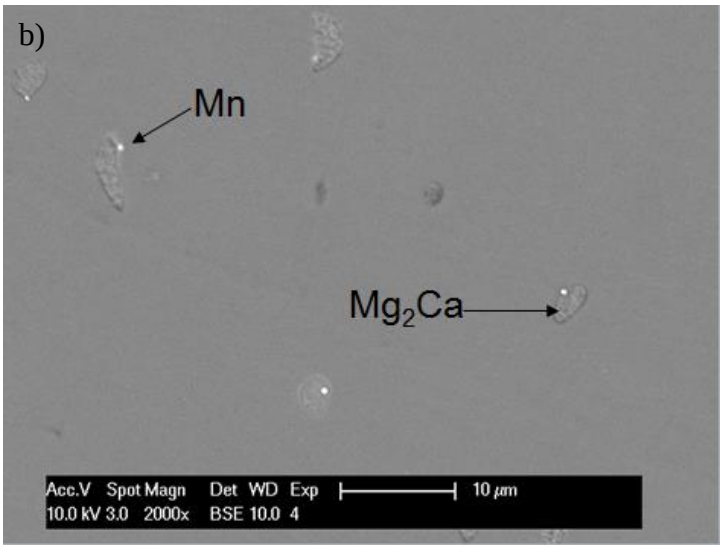

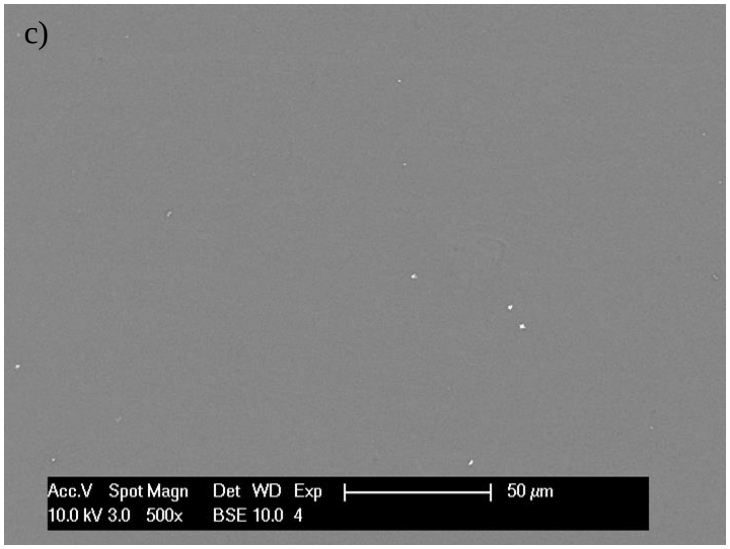

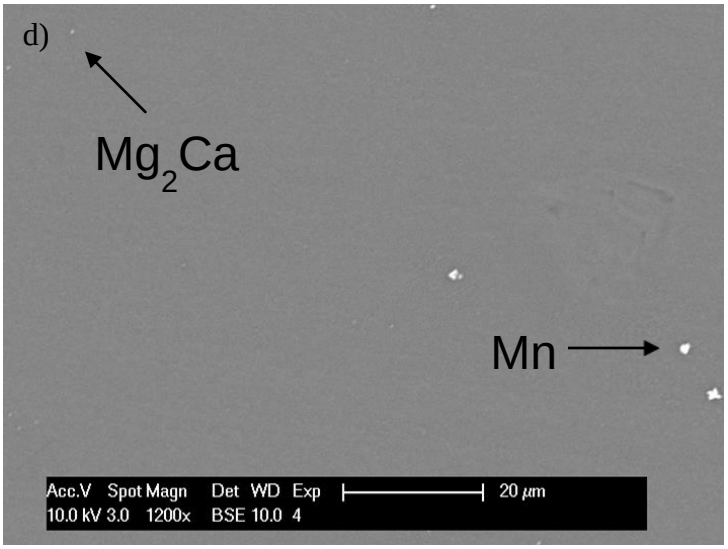

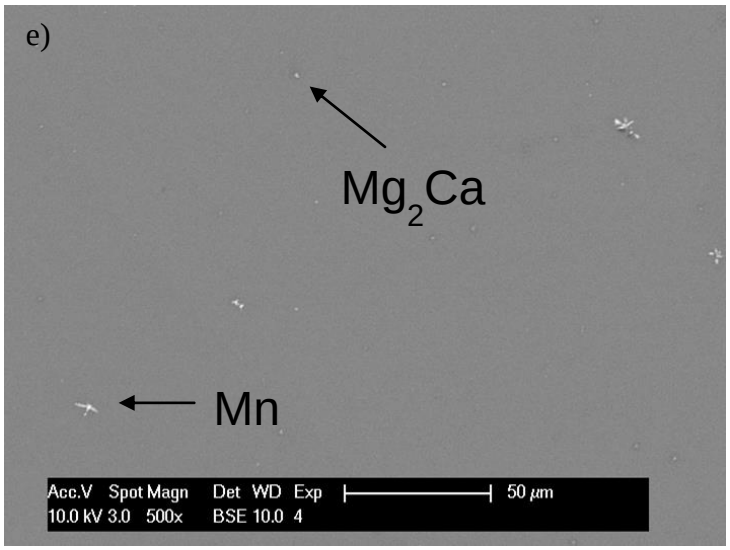

Figure 38: SEM images of:
a) and b) Mg 0.45Ca 1.82Mn; c) and d) Mg 0.21Ca 1.05Mn; e) Mg 0.17Ca 1.10Mn

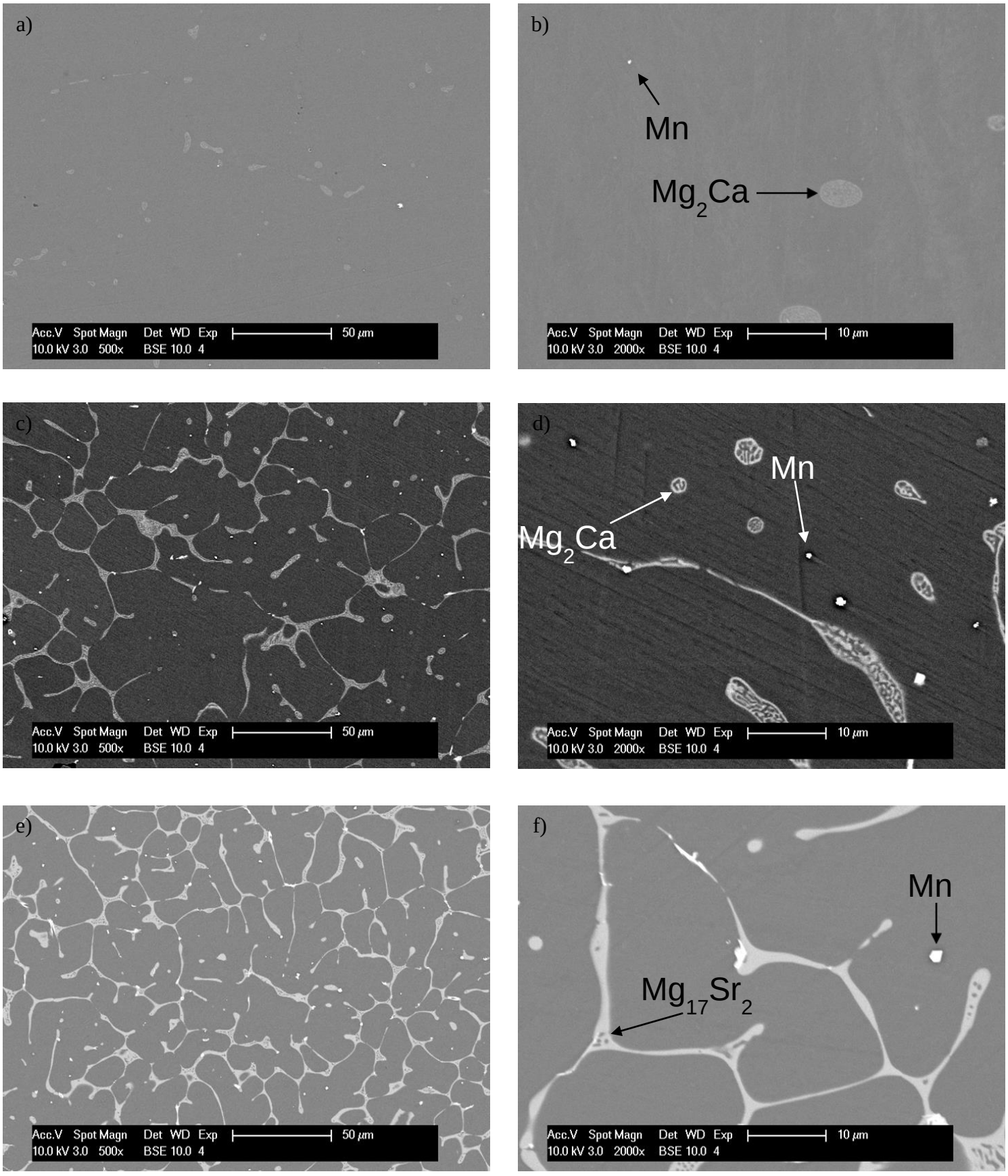

Figure 39: SEM images of a) and b) Mg 0.52Ca 0.62Mn; c) and d) Mg 1.49Ca 0.51Mn; e) and f) Mg 0.51Mn 0.86Sr

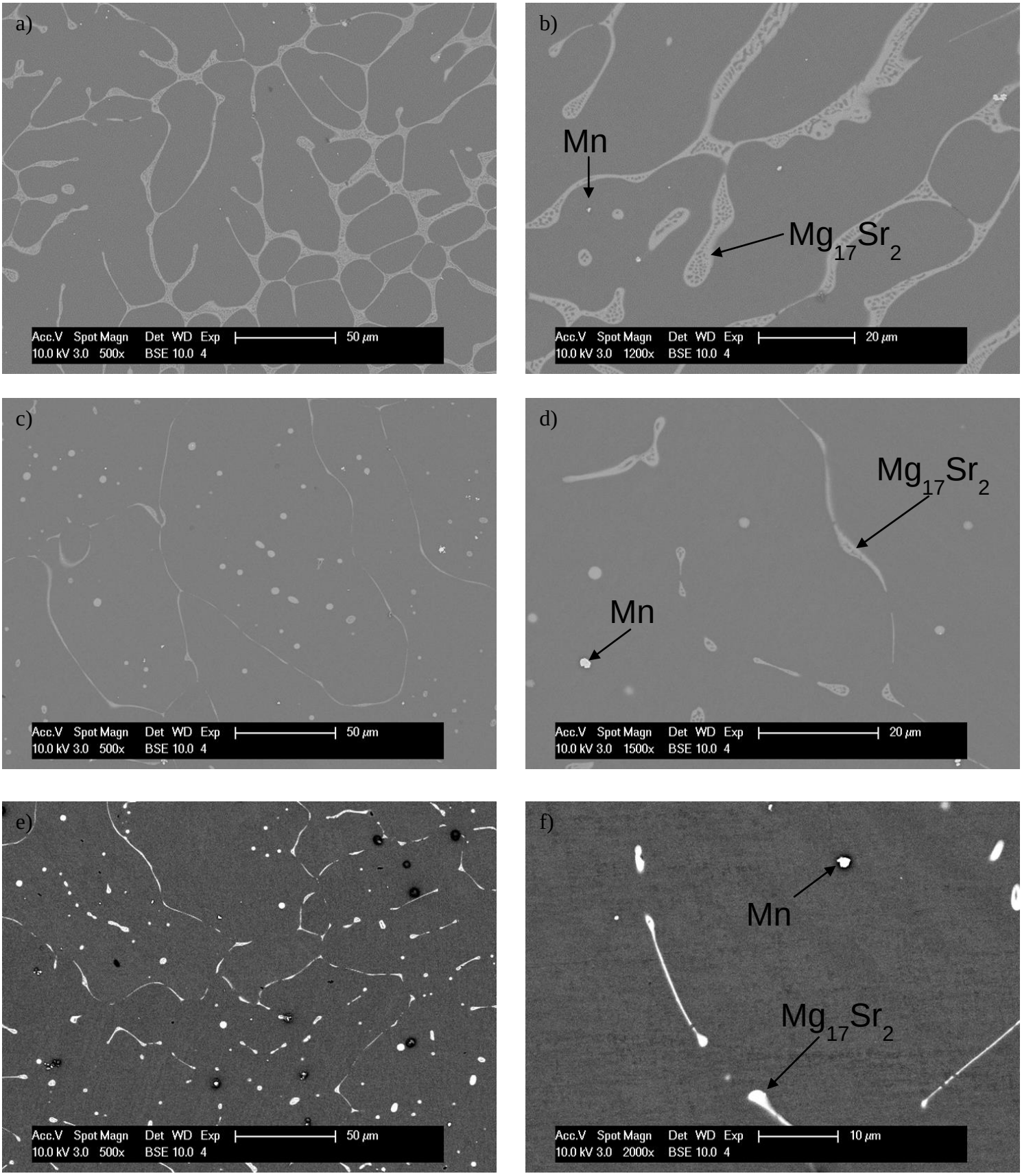

Figure 40: SEM images of a) and b) Mg 0.64Mn 0.65Sr;
c) and d) Mg 1.27Mn 0.11Sr; e) and f) Mg 1.86Mn 0.10Sr

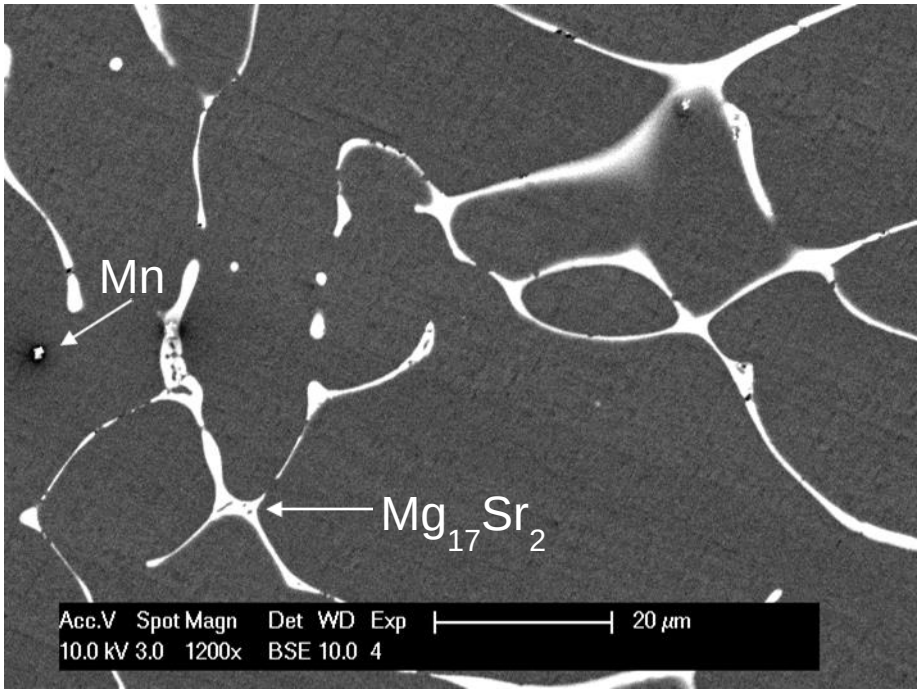

Figure 41: SEM image of Mg 0.73Mn 0.28Sr

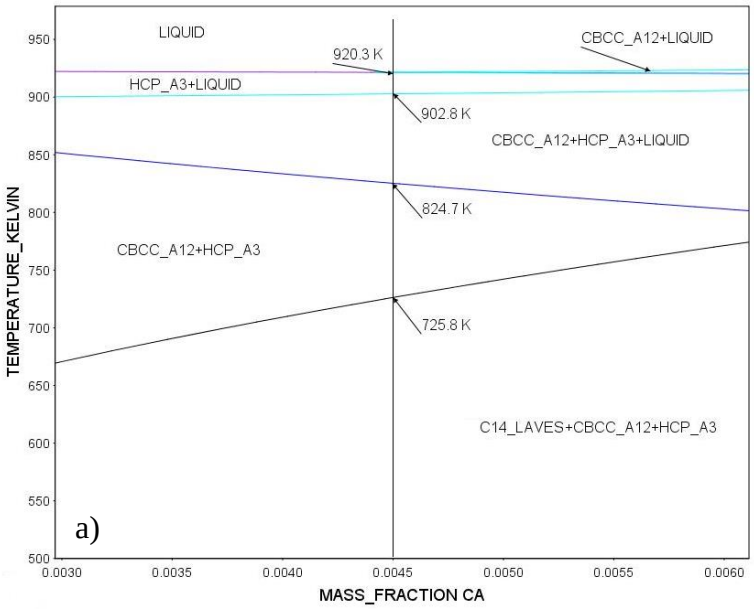

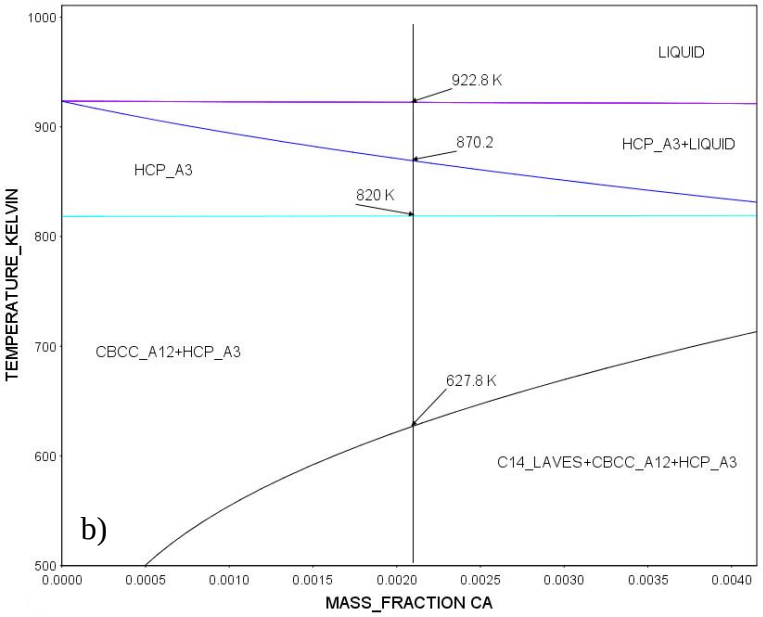

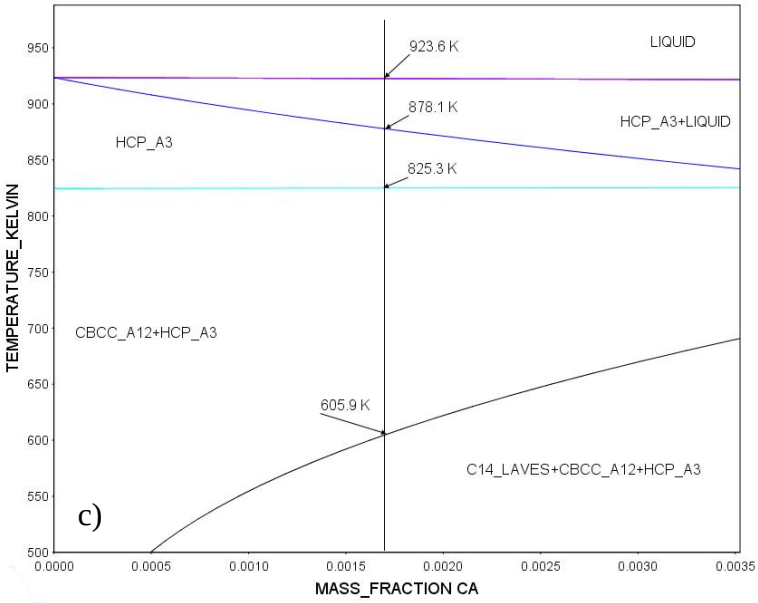

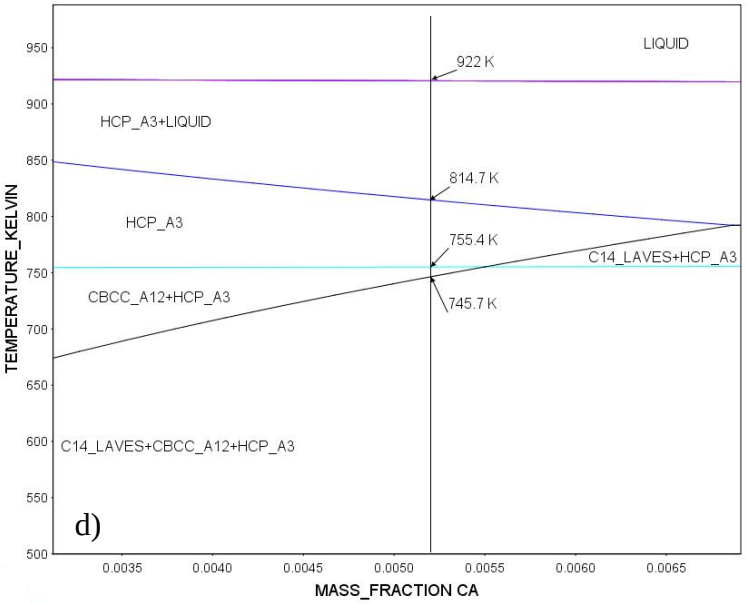

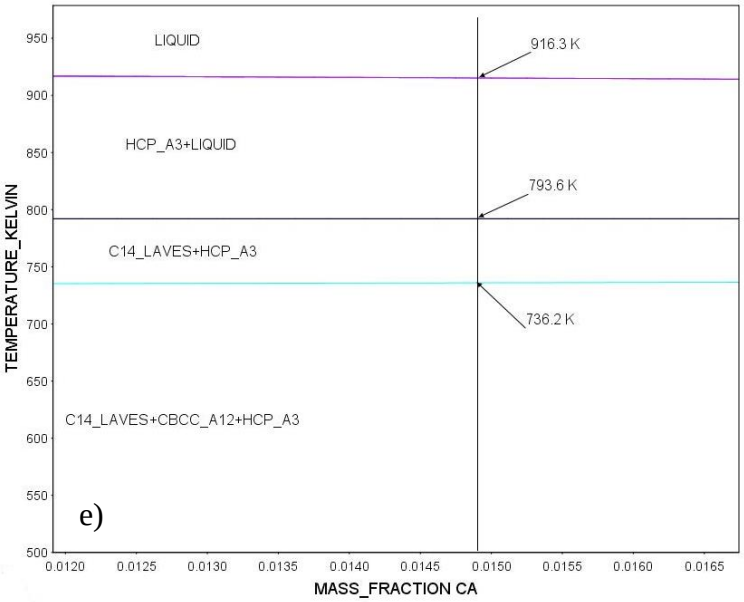

Figure 42: Vertical sections and solidification paths for the Mg-Ca-Mn system samples: a) Mg 0.45Ca 1.82Mn; b) Mg 0.21Ca 1.05Mn; c) Mg 0.17Ca 1.10Mn; d) Mg 0.52Ca 0.62Mn; e) Mg 1.49Ca 0.51Mn

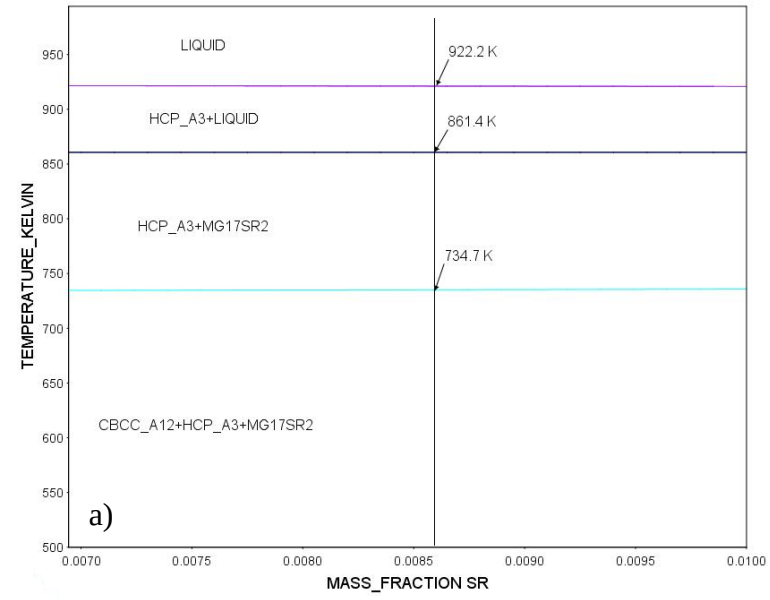

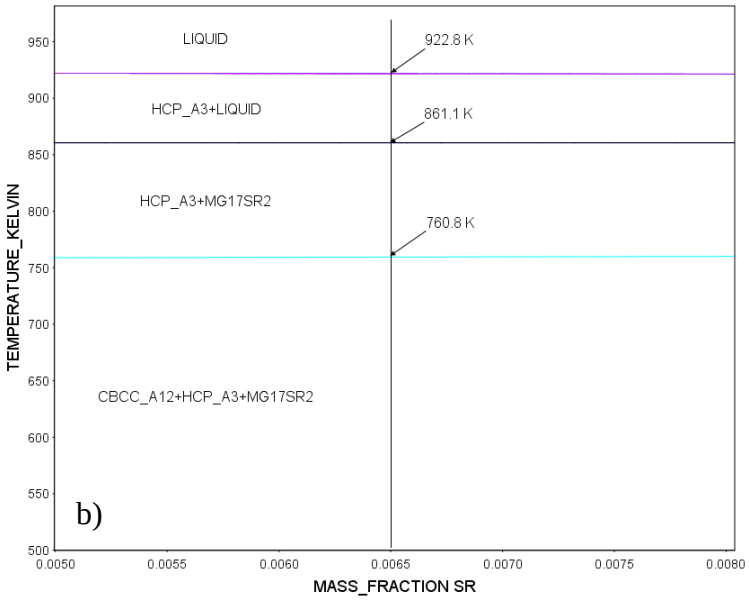

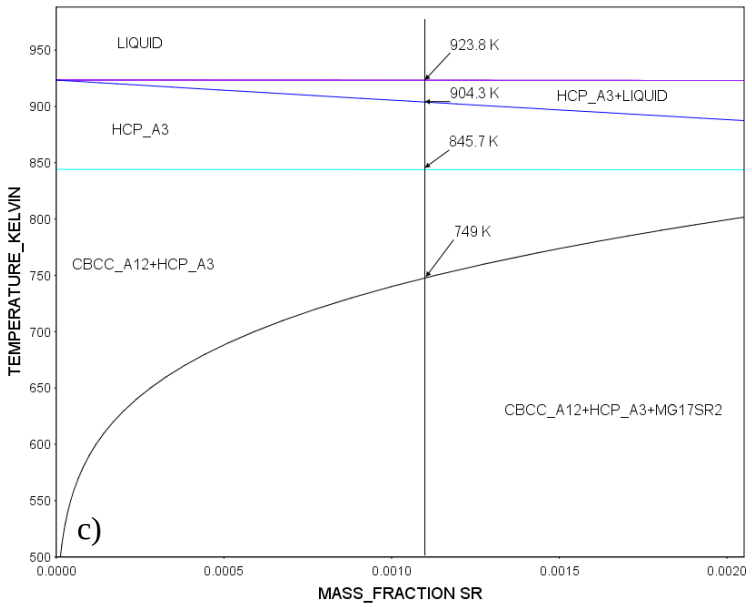

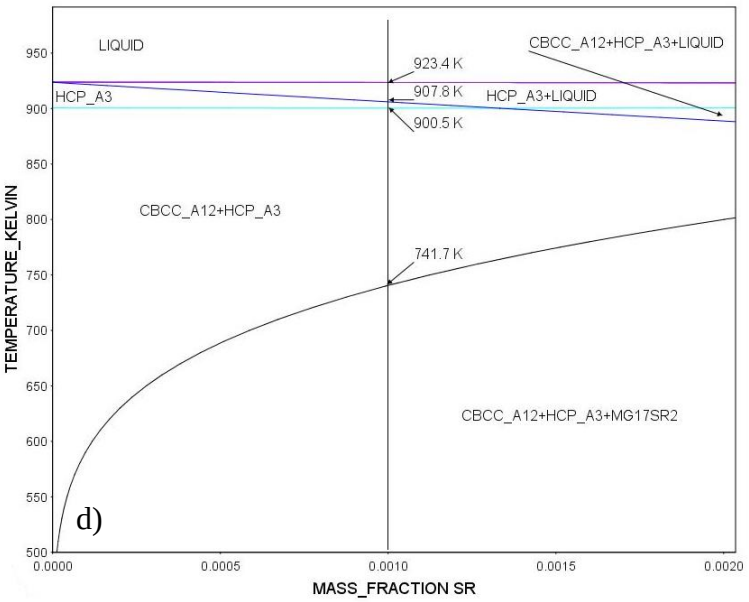

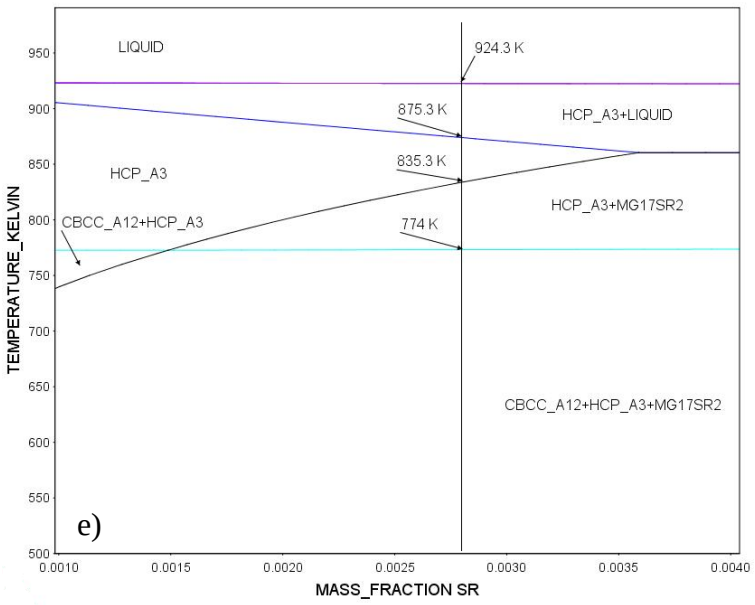

Figure 43: Vertical sections and solidification paths for the Mg-Mn-Sr system samples: a) Mg 0.51Mn 0.86Sr; b) Mg 0.64Mn 0.65Sr; c) Mg 1.27Mn 0.11Sr; d) Mg 1.86Mn 0.10Sr; e) Mg 0.73Mn 0.28Sr

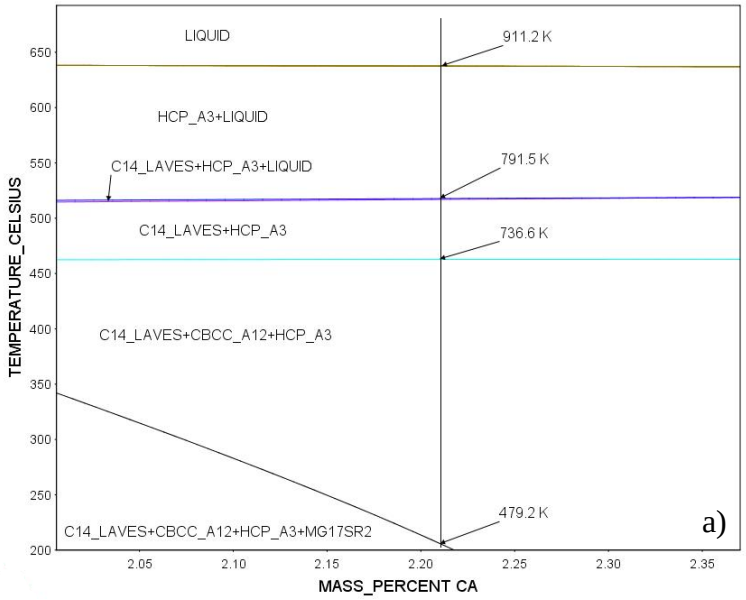

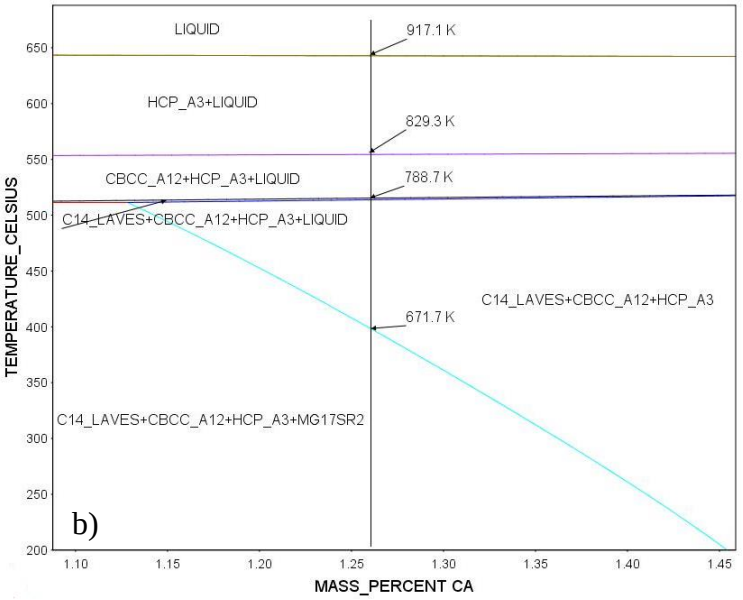

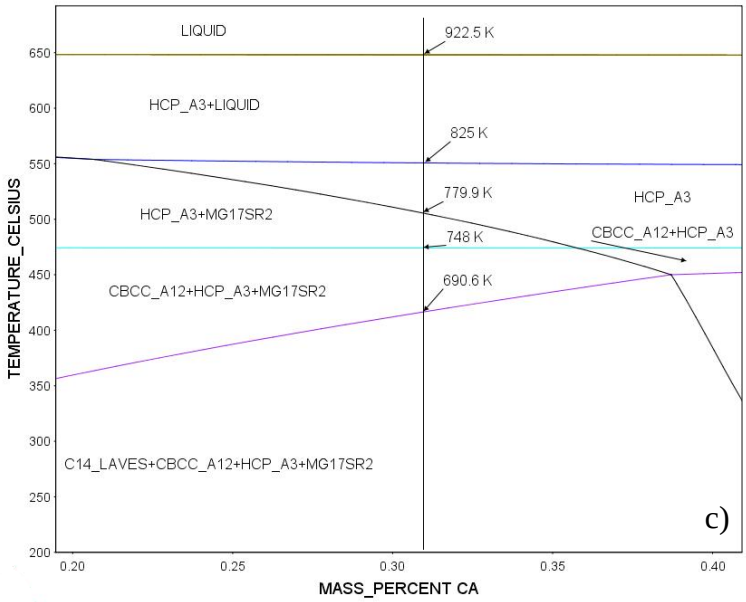

Figure 44: Vertical sections and solidification paths for the Mg-Ca-Mn-Sr system samples: a) Mg 2.21Ca 0.50Mn 0.17Sr; b) Mg 1.26Ca 1.06Mn 0.30Sr; c) Mg 0.31Ca 0.58Mn 0.16Sr

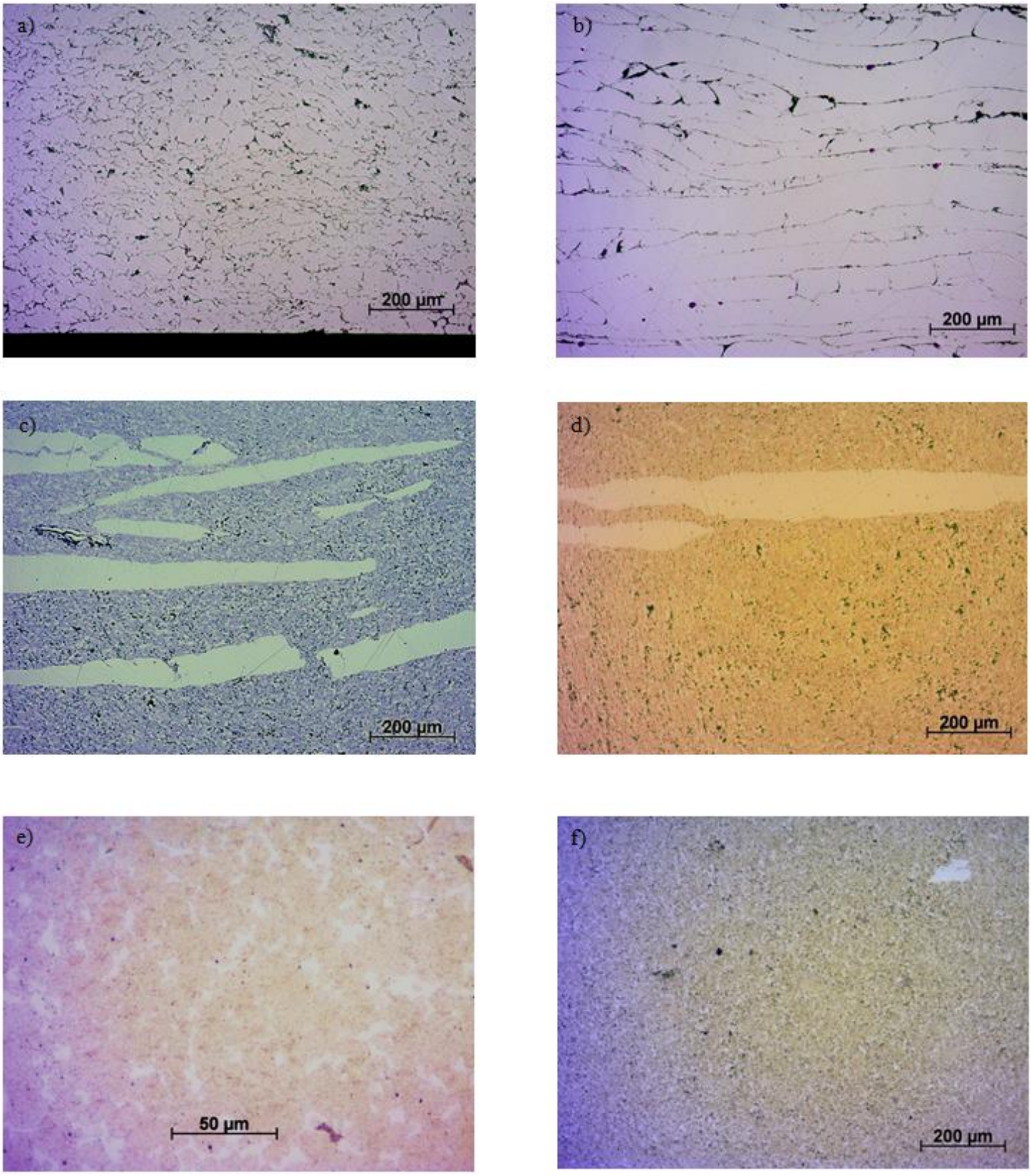

Figure 45: Microstructure images of samples manufactured via SPS after the following milling times: a) 0h (no milling); b) 1h; c) 6h; d)13h; e)18h; f)20h

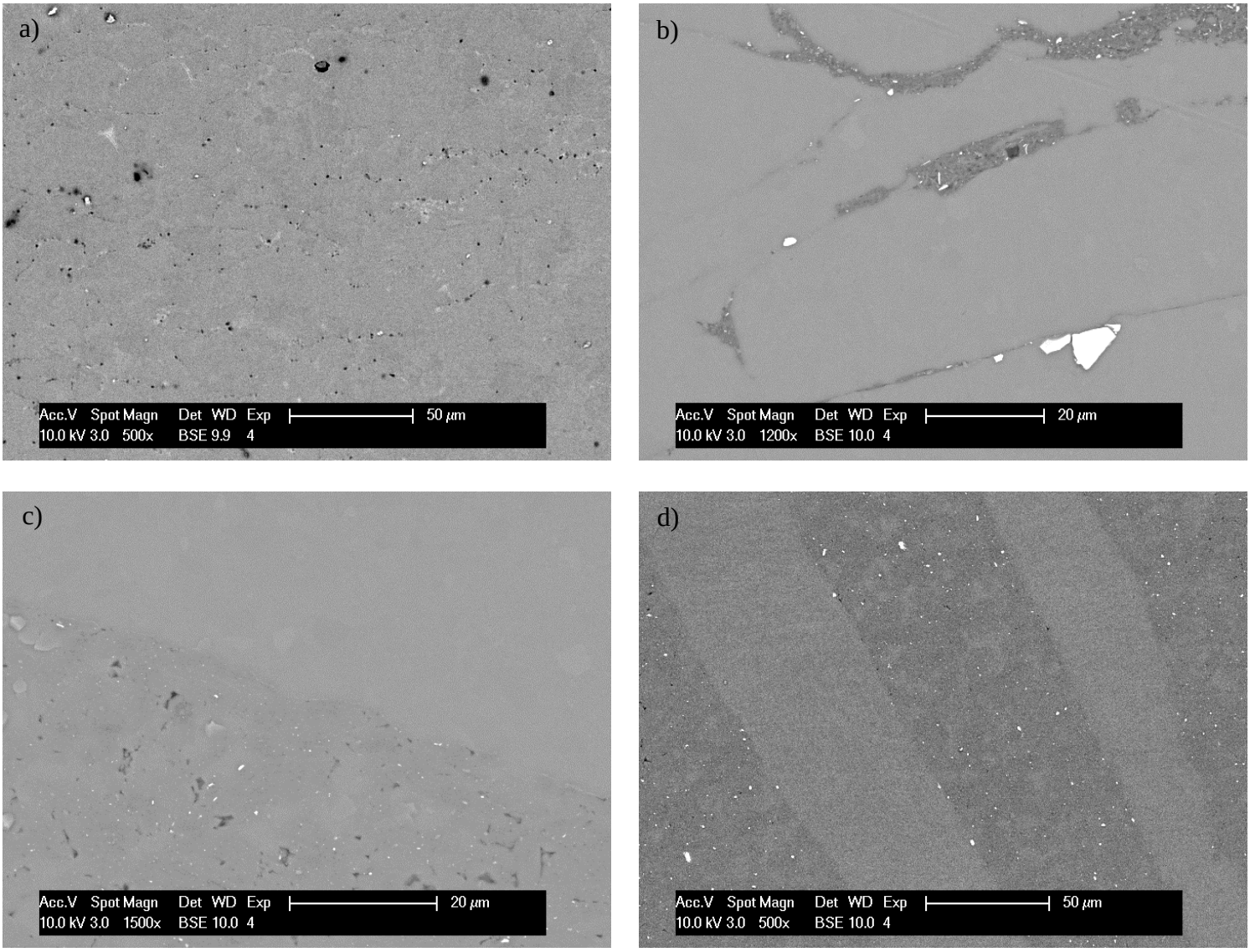

Figure 46: SEM micrographs of samples manufactured via SPS after the following milling times: a) 0h (no milling); b) 1h; c) 6h; d)13h

Table 14. Powder order

Element	Company	Purity	Size	Quantity	Price	Reference
Mg	ABCR	99.8%	45µm	100g	55.1€	*1
	Alfa Aesar	99.8%	45µm	100g	61.5€	
	Alfa Aesar	99.8%	45µm	500g	161€	
	Chempur	99.99%	4x4mm	100g	70.6€	
	Chempur	99%	315-630µm	1kg	110€	
Mn	Chempur	99.95%	45µm	50g	91€	*2
	ABCR	99.95%	45µm	25g	71.6€	*3
	Alfa Aesar	99.95%	45µm	25g	71.6€	*4
	Chempur	99.99%	0.8-3mm	50g	98.5€	
Ca	Alfa Aesar	99.5%	1.18mm	10g/50g	24€/60€	*5
	Chempur	99.5%	3.35mm	100g	125€	
Sr	Sigma Aldrich	99%	Granular	25g	172.5€	403326-25G
	Chempur	99.2%	<8mm	25g	596€	901991-25
	Chempur	99%	<20mm	50g	158.5€	009416-50
	Alfa Aesar	99.95%	Dendrites	5g	634€	*6
	Alfa Aesar	99.8%	Dendrites	5g	664€	*7
Si	H.C.Starck	99.995%	<8µm			*8
	Chempur	99.999%	45µm	50g	115€	*9
	ABCR	99.999%	45µm	25g	89€	*10
	Alfa Aesar	99.999%	45µm	1g/10g	24.8€/72.8€	*11
	Alfa Aesar	99.999%	45µm	10g	69.4€	*12

*1: http://www.abcr.de/shop/en/Magnesium-powder-325-mesh-99-8-198015.html/
*2: Article no.: 009255-50 product: Manganese Powder -325 mesh/ 99.95% CAS no.: [7439-96-5]
*3: http://www.abcr.de/shop/de/Manganese-powder-325-mesh-99-95-metals-basis-218227.html/
*4: http://www.alfa.com/en/catalog/36315
*5: http://www.alfa.com/en/catalog/42917
*6: http://www.alfa.com/en/catalog/38624
*7: http://www.alfa.com/en/catalog/42929
*8: http://www.hcstarck.com/hcs-admin/file/8a8181e225548334012554ce05db17e4.de.0/Advanced_Ceramic_Powders_0614_HC_Starck.pdf
*9: article no.: 903036-50 product: Silicon Powder -100, +325 mesh, amorphous/ 99.999% CAS no.: [7440-21-3]
*10: http://www.abcr.de/shop/de/Silicon-powder-99-999-325-mesh-63413.html/
*11: http://www.alfa.com/en/catalog/35662
*12: http://www.alfa.com/en/catalog/46654